

Quadratic response theory of the energy loss of charged particles in an electron gas

J. M. Pitarke

Materia Kondentsatuaren Fisika Saila, Zientzi Falkultatea, Euskal Herriko Unibertsitatea, 644 Posta kutxatila, 48080 Bilbo, Basque Country, Spain

R. H. Ritchie

Oak Ridge National Laboratory, P.O. Box 2008, Oak Ridge, Tennessee 37831-6123

P. M. Echenique

Materialen Fisika Saila, Kimika Falkultatea, Euskal Herriko Unibertsitatea, 1072 Posta kutxatila, 20080 Donostia, Basque Country, Spain

(Received 28 March 1995; revised manuscript received 17 May 1995)

A quadratic response theory of the energy loss of charged particles in matter is developed, following a diagrammatic analysis of the many-body interactions between a moving charge and the electron gas. The linear and quadratic density response functions of the medium are evaluated in the random-phase approximation (RPA), and a result for the stopping power is obtained, up to third order in the ion charge, Z_1e , for a wide range of particle velocities. The low- and high-velocity limits of the full RPA result are also studied, and a local plasma approximation is used to show that our calculations are in good agreement with measurements of the energy loss of protons and antiprotons in silicon.

I. INTRODUCTION

It is well known that the Bethe quantal theory of the electronic stopping power of matter for moving charged particles,¹ which is based on the first Born approximation, yields a result that is proportional to the square of the projectile charge, Z_1e . At lower velocities, where the Born approximation becomes suspect, the transition to classical scattering, treated by Bloch,² results in a correction term that does not depend on the sign of Z_1e . However, the measurements of Barkas *et al.*³ revealed differences between the ranges of positive and negative pions with the same energy, showing that the stopping power exhibits a dependence on the sign of the projectile charge. This dependence was later investigated by comparing measured stopping powers for proton, α particles, and lithium nuclei,^{4,5} and, more recently, for protons and antiprotons,^{6,7} extracting, therefore, the contribution to the energy loss that is proportional to Z_1^3 after assuming that other terms proportional to odd powers of Z_1 are negligible in the velocity regimes under study.

Ashley, Ritchie, and Brandt⁸ evaluated the contribution to the stopping power that is proportional to Z_1^3 , applying perturbation theory to the Bohr semiclassical harmonic-oscillator model of the atom.⁹ Since then, quantal calculations of the so-called Z_1^3 effect using an electron gas model and also a harmonic-oscillator model of the target have been performed by several authors.¹⁰⁻¹⁹ The first rigorous many-body perturbation-theoretic calculation of the Z_1^3 correction in the full random-phase approximation (RPA) for an

electron gas, for arbitrary nonrelativistic velocities of the projectile, has been reported only very recently.²⁰ For reviews of the experimental and theoretical situation see Refs. 17, 21, 22.

In this paper we investigate the Z_1^3 correction to the stopping power of an electron gas for ions, in the full RPA. In Sec. II, a diagrammatic analysis of the scattering matrix elements corresponding to processes leading to all possible momentum transfers to the electron gas is made, following procedures of many-body perturbation theory, and the terms of first and second order in the ion charge are extracted; this analysis allows us to give an interpretation of the different processes involved. In Sec. III, the linear and quadratic density response functions, represented in terms of double and triple vertex functions, are considered, the imaginary part of the triple vertex function is evaluated analytically in the RPA, and is expressed in terms of a sum over hole and particle states. This result is used in Sec. IV to derive an explicit expression for the Z_1^3 correction to the stopping power formula in terms of both the real and the imaginary part of double and triple vertex functions, and the low- and high-velocity limits are also discussed. In Sec. V, numerical calculations of the Z_1^3 effect are presented, as a function of the velocity of the penetrating particle, the range of validity of the previously studied low- and high-velocity limits is analyzed, and a local plasma approximation is used in order to compare our results with those deduced from experimental data on energy loss by protons and antiprotons in silicon.⁶ In Sec. VI, our conclusions are presented.

II. SCATTERING MATRIX: DIAGRAMMATIC ANALYSIS

We consider an electron gas of density n through which an ion of charge Z_1e and velocity \mathbf{v} passes. Treating the heavy particle as a prescribed source of energy and momentum, let the electron gas be described by an isotropic homogeneous assembly of electrons immersed in a uniform background of positive charge and volume Ω , and take an externally applied potential on an electron at \mathbf{r} due to the field of the penetrating particle:

$$u(\mathbf{r}, t) = -\frac{Z_1 e^2}{|\mathbf{r} - \mathbf{v}t|}. \quad (2.1)$$

The scattering matrix can be written as a time-ordered exponential²³

$$S = T \left\{ \exp \left[-i\hbar^{-1} \int_{-\infty}^{\infty} dt e^{-\eta|t|} H_I'(t) \right] \right\}, \quad (2.2)$$

where T is the chronological operator, which indicates that the product to be integrated must be time ordered, and $H_I'(t)$ represents the perturbing Hamiltonian in the interaction picture, which has been assumed to be initially zero and slowly switched on. η is a positive infinitesimal.

In the representation of second quantization, the perturbing Hamiltonian reads, in the interaction picture

$$\begin{aligned} H_I'(t) &= \int d^3r \psi^\dagger(x) u(x) \psi(x) \\ &+ \frac{1}{2} \int d^3r \int d^4x' \psi^\dagger(x) \psi^\dagger(x') v(x, x') \psi(x') \psi(x) \\ &+ H_I^{\text{BG}}(t). \end{aligned} \quad (2.3)$$

H^{BG} represents the interaction between the electron gas and the positive background, $u(x)$, with $x = (\mathbf{r}, t)$, is the electron-heavy ion interaction potential of Eq. (2.1), $v(x, x')$ represents the electron-electron instantaneous Coulomb interaction, and $\psi(x)$ and $\psi^\dagger(x)$ are field operators in the interaction picture destroying and creating, respectively, a particle at the point \mathbf{r} at time t :

$$\psi(x) = \sum_i e^{-i\omega_i t} \phi_i(\mathbf{r}) a_i \quad (2.4)$$

and

$$\psi^\dagger(x) = \sum_i e^{i\omega_i t} \phi_i^*(\mathbf{r}) a_i^\dagger, \quad (2.5)$$

where a_i and a_i^\dagger are annihilation and creation operators for fermions, and $\phi_i(\mathbf{r})$ represents a complete set of orthonormal single-particle wave functions satisfying the time-independent Schrödinger equation with energy $\hbar\omega_i$; for a homogeneous electron gas, these wave functions can be taken to be momentum eigenfunctions.

The matrix element

$$S_{f,i} = \frac{\langle \Phi_0 | a_f S a_i^\dagger | \Phi_0 \rangle}{\langle \Phi_0 | S | \Phi_0 \rangle}, \quad (2.6)$$

corresponding to the process of carrying the system from an initial state $a_i^\dagger |\Phi_0\rangle$ to a final state $a_f^\dagger |\Phi_0\rangle$, $|\Phi_0\rangle$ being the vacuum state, can be expanded with respect to the coupling constant e^2 after introduction of the Hamiltonian of Eq. (2.3) into Eq. (2.2). Then, one can apply Wick's theorem, noting that only normal ordered products with two uncontracted operators contribute, and an expression for the matrix element can be obtained.

It is well known that for a homogeneous electron gas, contributions from the uniform positive background are canceled by the sum of the so-called "tadpole" contributions where the average electron density in the unperturbed ground state,

$$\rho^0(x) = -\langle \Phi_0 | T[\psi(x) \psi^\dagger(x)] | \Phi_0 \rangle, \quad (2.7)$$

is involved. On the other hand,

$$G^0(x, x') = -i \langle \Phi_0 | T[\psi(x) \psi^\dagger(x')] | \Phi_0 \rangle \quad (2.8)$$

represents the free particle propagator, and

$$\langle \Phi_0 | a_f \psi^\dagger(x) \psi(x') a_i^\dagger | \Phi_0 \rangle = e^{i\omega_f t} \phi_f^*(\mathbf{r}) e^{-i\omega_i t'} \phi_i(\mathbf{r}'). \quad (2.9)$$

Consequently, after introduction of standard Fourier integral representations of the quantities involved and taking $\phi_i(\mathbf{r})$ and $\phi_f(\mathbf{r})$ to be plane-wave states of momentum \mathbf{s} and \mathbf{p} , respectively, we find, up to second order in the ion charge:

$$\begin{aligned} S_{f,i} &= \frac{1}{\Omega} (-i\hbar^{-1}) \int d^4q \delta^4(q + s - p) \mathcal{U}_q [1 + g_1(s, p)] \\ &+ \frac{i}{\Omega} (-i\hbar^{-1})^2 \int d^4q \delta^4(q + s - p) \int \frac{d^4q_1}{(2\pi)^4} \mathcal{U}_{q_1} \mathcal{U}_{q-q_1} G_{s+q_1}^0 [1 + g_2(s, p, q_1)] \\ &+ \frac{1}{\Omega} (-i\hbar^{-1})^3 \int d^4q \delta^4(q + s - p) \mathcal{V}_q \int \frac{d^4q_1}{(2\pi)^4} \mathcal{U}_{q_1} \mathcal{U}_{q-q_1} M_{q, q_1} [1 + g_1(s, p)], \end{aligned} \quad (2.10)$$

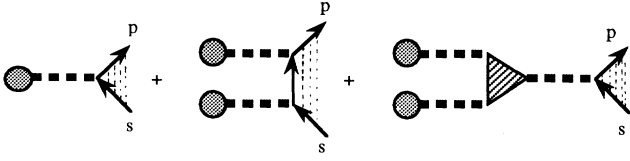


FIG. 1. Diagrammatic representation of the matrix element of Eq. (2.10). In the first diagram a full dashed line, representing a screened Coulombic interaction, leads from an external point corresponding to the external source of momentum and energy to a dressed fermion-scattering vertex. Solid internal lines in the second and third diagrams are zero-order propagators, and the dressed triple internal vertex represents the exact quadratic density response function of the medium.

which can be represented diagrammatically as in Fig. 1. Here, $s = (\mathbf{s}, \omega_s)$ and $p = (\mathbf{p}, \omega_p)$, with $\omega_{\mathbf{k}} = \hbar \mathbf{k}^2 / (2m_e)$, and \mathcal{U}_q and \mathcal{V}_q , represented in Fig. 1 by full dashed lines, are screened interaction potentials in the momentum representation (see Fig. 2):

$$\mathcal{U}_q = -2\pi Z_1 \delta(q^0 - \mathbf{q} \cdot \mathbf{v}) \mathcal{V}_q \quad (2.11)$$

and

$$\mathcal{V}_q = v_{\mathbf{q}} + v_{\mathbf{q}} \chi_q \mathcal{V}_q, \quad (2.12)$$

or

$$\mathcal{V}_q = \epsilon_q^{-1} v_{\mathbf{q}}, \quad (2.13)$$

where $v_{\mathbf{q}}$ is the Fourier transform of the electron-electron bare Coulomb interaction

$$v_{\mathbf{q}} = \frac{4\pi e^2}{\mathbf{q}^2}, \quad (2.14)$$

and ϵ_q represents the dielectric function of the medium

$$\epsilon_q = (1 + v_{\mathbf{q}} \chi_q)^{-1}. \quad (2.15)$$

χ_q , represented in Fig. 2 by a dressed double vertex, is the exact so-called linear density response function of the medium, M_{q,q_1} , represented in Fig. 1 by a dressed triple vertex, is the exact quadratic density response function of the medium, and G_q^0 is the Fourier transform of the free particle propagator of Eq. (2.8):

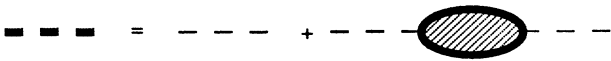


FIG. 2. The screened Coulombic interaction, represented by a full dashed line, is obtained from the exact linear density response function of the medium, represented by a dressed double internal vertex, according to Eq. (2.12).

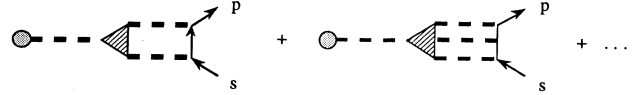


FIG. 3. Vertex ladder contributions to the matrix element $S_{f,i}$, which have been neglected in Eq. (2.10).

$$G_q^0 = \frac{1 - n_{\mathbf{q}}}{q^0 - \omega_{\mathbf{q}} + i\eta} + \frac{n_{\mathbf{q}}}{q^0 - \omega_{\mathbf{q}} - i\eta}, \quad (2.16)$$

where

$$n_{\mathbf{q}} = \theta(q_F - |\mathbf{q}|) \quad (2.17)$$

represents the occupation number, q_F being the Fermi momentum, and $\theta(x)$, the Heaviside function.

Vertex ladder contributions to the matrix element, represented diagrammatically in Fig. 3, have been neglected in Eq. (2.10), and all self-energy and vertex insertions, included in the dressed vertices of Fig. 1, are introduced in Eq. (2.10) by means of $g_1(s, p)$ and $g_2(s, p, q_1)$.

The first diagram in Fig. 1, represented by a full dashed line leading from an external point to a dressed fermion-scattering vertex, describes a process in which an electron-hole pair is generated in the electron gas by the screened ion potential, while the second and third diagrams correspond to the excitation of an electron-hole pair by the penetrating charged particle, which is assumed to interact twice with the electron gas. The second diagram represents the process in which an electron or hole scatters twice from the screened potential, and the third diagram corresponds to the excitation of an electron-hole pair through two virtual excitations that combine via a triple vertex into a single screened interaction; we refer to this as a quadratically screened interaction.

The matrix element

$$S_{f_1 f_2, i_1 i_2} = \frac{\langle \Phi_0 | a_{f_1} a_{f_2} S a_{i_1}^\dagger a_{i_2}^\dagger | \Phi_0 \rangle}{\langle \Phi_0 | S | \Phi_0 \rangle}, \quad (2.18)$$

corresponding to the process of carrying the system from an initial state $a_{i_1}^\dagger a_{i_2}^\dagger | \Phi_0 \rangle$ to a final state $a_{f_1}^\dagger a_{f_2}^\dagger | \Phi_0 \rangle$, can be expanded by noting that only normal ordered products with four uncontracted field operators contribute, and matrix elements for processes involving higher-order excitations can be derived in a similar way.

III. LINEAR AND QUADRATIC RESPONSE FUNCTIONS IN THE RPA

In the so-called random-phase approximation, the exact linear density response function, χ_q , is approximated by summing over all ringlike diagrams, as shown in Fig. 4. In this approximation all self-energy and vertex insertions are neglected, and we also replace, therefore, the exact quadratic density response function M_{q,q_1} by the empty triple vertex, and the dressed scattering vertices



FIG. 4. Diagrammatic representation of the RPA linear density response function χ_q approximated by summing over the infinite set of diagrams containing a string of empty bubbles.

of Fig. 1 by the corresponding undressed ones. Thus, $g_1(s, p)$ and $g_2(s, p, q_1)$ are set equal to zero in Eq. (2.10), and, on the other hand, one can write

$$\chi_q = \chi_q^0 + \chi_q^0 v_q \chi_q \quad (3.1)$$

and

$$\epsilon_q = 1 - \chi_q^0 v_q, \quad (3.2)$$

where χ_q^0 is the linear density response function of the noninteracting electron gas

$$\chi_q^0 = -2i\hbar^{-1} \int d^4k G_k^0 G_{k+q}^0 \quad (3.3)$$

and

$$M_{q, q_1} = 2i \int \frac{d^4k}{(2\pi)^4} G_k^0 G_{k+q}^0 G_{k+q_1}^0. \quad (3.4)$$

After carrying out the integration of Eq. (3.3) over the frequency component of k , k^0 , one finds

$$\chi_q^0 = 2\hbar^{-1} \int \frac{d^3\mathbf{k}}{(2\pi)^3} \left[\frac{n_{\mathbf{k}}(1 - n_{\mathbf{k}+\mathbf{q}})}{q^0 - (\omega_{\mathbf{k}+\mathbf{q}} - \omega_{\mathbf{k}}) + i\eta} - \frac{(1 - n_{\mathbf{k}})n_{\mathbf{k}+\mathbf{q}}}{q^0 + (\omega_{\mathbf{k}} - \omega_{\mathbf{k}+\mathbf{q}}) - i\eta} \right], \quad (3.5)$$

and noticing that both, $i\eta$ in the first denominator and $-i\eta$ in the second one, can be written as $i\eta_q = i\eta \text{sgn}(q^0)$, the occupation numbers sum up to give

$$\chi_q^0 = 2\hbar^{-1} \int \frac{d^3k}{(2\pi)^3} n_{\mathbf{k}} \left[\frac{1}{q^0 + \omega_{\mathbf{k}} - \omega_{\mathbf{k}+\mathbf{q}} + i\eta_q} - \frac{1}{q^0 - \omega_{\mathbf{k}} + \omega_{\mathbf{k}+\mathbf{q}} + i\eta_q} \right]. \quad (3.6)$$

The integrals in Eq. (3.6) can be evaluated quite straightforwardly, and the time-ordered function of Hubbard²⁴ is obtained, which is an even function of q^0 and coincides for positive values of q^0 with the well-known retarded function of Lindhard.²⁵

As far as the imaginary part of χ_q^0 is concerned, the symbolic identity

$$\lim_{\eta \rightarrow 0^+} \frac{1}{x \pm i\eta} = \text{P} \frac{1}{x} \mp i\pi\delta(x) \quad (3.7)$$

can be used, P standing for principal value, to conclude that $\text{Im}\chi_q^0$ can be represented in terms of a sum over hole and particle states, as follows:²⁶

$$\begin{aligned} \text{Im}\chi_q^0 &= -(2\pi)^4 \hbar^{-1} \int \frac{d^3s}{(2\pi)^3} n_{\mathbf{s}} \\ &\times \int \frac{d^3p}{(2\pi)^3} (1 - n_{\mathbf{p}}) \delta^3(\mathbf{q} + \mathbf{s} - \mathbf{p}) \\ &\times [\delta(q^0 + \omega_{\mathbf{s}} - \omega_{\mathbf{p}}) + \delta(q^0 - \omega_{\mathbf{s}} + \omega_{\mathbf{p}})]. \end{aligned} \quad (3.8)$$

In order to evaluate the three-point function of Eq. (3.4), we carry out, first of all, the integration over k^0 in the complex plane by always closing the integration path on the side that displays fewer singularities, and find:

$$\begin{aligned} M_{q, q_1} &= -2 \int \frac{d^3k}{(2\pi)^3} \left[\frac{n_{\mathbf{k}}(1 - n_{\mathbf{k}+\mathbf{q}})(1 - n_{\mathbf{k}+\mathbf{q}_1})}{(q^0 + \omega_{\mathbf{k}} - \omega_{\mathbf{k}+\mathbf{q}} + i\eta)(q_1^0 + \omega_{\mathbf{k}} - \omega_{\mathbf{k}+\mathbf{q}_1} + i\eta)} \right. \\ &\quad - \frac{(1 - n_{\mathbf{k}})n_{\mathbf{k}+\mathbf{q}}n_{\mathbf{k}+\mathbf{q}_1}}{(q^0 + \omega_{\mathbf{k}} - \omega_{\mathbf{k}+\mathbf{q}} - i\eta)(q_1^0 + \omega_{\mathbf{k}} - \omega_{\mathbf{k}+\mathbf{q}_1} - i\eta)} \\ &\quad + \frac{n_{\mathbf{k}+\mathbf{q}}(1 - n_{\mathbf{k}})(1 - n_{\mathbf{k}+\mathbf{q}_1})}{(-q^0 + \omega_{\mathbf{k}+\mathbf{q}} - \omega_{\mathbf{k}} + i\eta)(-q_1^0 + \omega_{\mathbf{k}+\mathbf{q}} - \omega_{\mathbf{k}+\mathbf{q}_1} + i\eta)} \\ &\quad - \frac{(1 - n_{\mathbf{k}+\mathbf{q}})n_{\mathbf{k}}n_{\mathbf{k}+\mathbf{q}_1}}{(-q^0 + \omega_{\mathbf{k}+\mathbf{q}} - \omega_{\mathbf{k}} - i\eta)(-q_1^0 + \omega_{\mathbf{k}+\mathbf{q}} - \omega_{\mathbf{k}+\mathbf{q}_1} - i\eta)} \\ &\quad + \frac{n_{\mathbf{k}+\mathbf{q}_1}(1 - n_{\mathbf{k}})(1 - n_{\mathbf{k}+\mathbf{q}})}{(-q_1^0 + \omega_{\mathbf{k}+\mathbf{q}_1} - \omega_{\mathbf{k}} + i\eta)(q^0 - q_1^0 + \omega_{\mathbf{k}+\mathbf{q}_1} - \omega_{\mathbf{k}+\mathbf{q}} + i\eta)} \\ &\quad \left. - \frac{(1 - n_{\mathbf{k}+\mathbf{q}_1})n_{\mathbf{k}}n_{\mathbf{k}+\mathbf{q}}}{(-q_1^0 + \omega_{\mathbf{k}+\mathbf{q}_1} - \omega_{\mathbf{k}} - i\eta)(q^0 - q_1^0 + \omega_{\mathbf{k}+\mathbf{q}_1} - \omega_{\mathbf{k}+\mathbf{q}} - i\eta)} \right]. \end{aligned} \quad (3.9)$$

Now, we follow the same argument leading from Eq. (3.5) to Eq. (3.6), and find, after some rearrangement, the

following result:

$$M_{q,q_1} = -2 \int \frac{d^3k}{(2\pi)^3} n_{\mathbf{k}} \left[\frac{1}{q^0 + \omega_{\mathbf{k}} - \omega_{\mathbf{k}+\mathbf{q}} + i\eta_q} \frac{1}{q_1^0 + \omega_{\mathbf{k}} - \omega_{\mathbf{k}+\mathbf{q}_1} + i\eta_{q_1}} \right. \\ \left. + \frac{1}{-q^0 + \omega_{\mathbf{k}} - \omega_{\mathbf{k}+\mathbf{q}} - i\eta_q} \frac{1}{-(q^0 - q_1^0) + \omega_{\mathbf{k}} - \omega_{\mathbf{k}+\mathbf{q}-\mathbf{q}_1} - i\eta_{q-q_1}} \right. \\ \left. + \frac{1}{-q_1^0 + \omega_{\mathbf{k}} - \omega_{\mathbf{k}+\mathbf{q}_1} - i\eta_{q_1}} \frac{1}{(q^0 - q_1^0) + \omega_{\mathbf{k}} - \omega_{\mathbf{k}-(\mathbf{q}-\mathbf{q}_1)} + i\eta_{q-q_1}} \right]. \quad (3.10)$$

Then, an analytical evaluation of the integrations involved gives, for the real part²⁷

$$\text{Re}M_{q,q_1} = -2 [I_{q,q_1} + I_{-q,-(q-q_1)} + I_{-q_1,q-q_1}], \quad (3.11)$$

where

$$I_{q,q_1} = \frac{m_e^2 \hbar^{-2}}{(2\pi)^2 |\mathbf{q}| |\mathbf{q}_1| \sin^2 \chi} \left[(A \cos \chi - A_1) \ln \left| \frac{A - q_F}{A + q_F} \right| + (A_1 \cos \chi - A) \ln \left| \frac{A_1 - q_F}{A_1 + q_F} \right| + I'_{q,q_1} \right], \quad (3.12)$$

$$I'_{q,q_1} = \begin{cases} -\sqrt{G^2 - q_F^2 \sin^2 \chi} \ln \left| \frac{AA_1 - q_F^2 \cos \chi + q_F \sqrt{G^2 - q_F^2 \sin^2 \chi}}{AA_1 - q_F^2 \cos \chi - q_F \sqrt{G^2 - q_F^2 \sin^2 \chi}} \right| & \text{for } G^2 - q_F^2 \sin^2 \chi \geq 0 \\ \sqrt{q_F^2 \sin^2 \chi - G^2} \left[2 \arccos \frac{AA_1 - q_F^2 \cos \chi}{\sqrt{(q_F^2 - A^2)(q_F^2 - A_1^2)}} - \pi |\text{sgn}(q^0) + \text{sgn}(q_1^0)| \right] & \text{for } G^2 - q_F^2 \sin^2 \chi \leq 0, \end{cases} \quad (3.13)$$

$$A = m \hbar^{-1} \frac{q^0}{|\mathbf{q}|} - \frac{|\mathbf{q}|}{2}, \quad (3.14)$$

$$A_1 = m \hbar^{-1} \frac{q_1^0}{|\mathbf{q}_1|} - \frac{|\mathbf{q}_1|}{2}, \quad (3.15)$$

and

$$G = \sqrt{A^2 - 2AA_1 \cos \chi + A_1^2}, \quad (3.16)$$

χ being the angle between \mathbf{q} and \mathbf{q}_1 . Although the appearance of the sign function in Eq. (3.13) may give rise to some discontinuities in I_{q,q_1} , $\text{Re}M_{q,q_1}$ is easily shown to be continuous, as pointed out in Ref. 27.

As far as the imaginary part of the triple vertex function is concerned, we take advantage, again, of the identity of Eq. (3.7), and find from Eq. (3.9) the following result:

$$\text{Im}M_{q,q_1} = H_{q,q_1} + H_{q_1,q} + H_{(q-q_1),-q_1}, \quad (3.17)$$

where H_{q,q_1} can be represented in terms of a sum over hole and particle states:

$$f_{q,q_1} = -\frac{m_e^2 \hbar^{-2}}{2\pi |\mathbf{q}| |\mathbf{q}_1| \sin^2 \chi} \left[(A \cos \chi - A_1) - \sqrt{G^2 - q_F^2 \sin^2 \chi} \text{sgn}(A \cos \chi - A_1) \theta(G^2 - q_F^2 \sin^2 \chi) \right] \theta(q_F - |A|). \quad (3.21)$$

$$H_{q,q_1} = (2\pi)^4 \text{P} \int \frac{d^3s}{(2\pi)^3} n_{\mathbf{s}} \int \frac{d^3p}{(2\pi)^3} (1 - n_{\mathbf{p}}) \delta^3(\mathbf{q} - \mathbf{p} + \mathbf{s}) \\ \times \left[\frac{\delta(q^0 + \omega_{\mathbf{s}} - \omega_{\mathbf{p}})}{q_1^0 + \omega_{\mathbf{s}} - \omega_{\mathbf{s}+\mathbf{q}_1}} \right. \\ \left. + \frac{\delta(q^0 - \omega_{\mathbf{s}} + \omega_{\mathbf{p}})}{-(q^0 - q_1^0) + \omega_{\mathbf{s}} - \omega_{\mathbf{s}+\mathbf{q}-\mathbf{q}_1}} \right], \quad (3.18)$$

and also as

$$H_{q,q_1} = 2\pi \text{sgn}(q^0) \text{P} \int \frac{d^3k}{(2\pi)^3} n_{\mathbf{k}} \left[\frac{\delta(q^0 + \omega_{\mathbf{k}} - \omega_{\mathbf{k}+\mathbf{q}})}{q_1^0 + \omega_{\mathbf{k}} - \omega_{\mathbf{k}+\mathbf{q}_1}} \right. \\ \left. - \frac{\delta(q^0 - \omega_{\mathbf{k}} + \omega_{\mathbf{k}+\mathbf{q}})}{-(q^0 - q_1^0) + \omega_{\mathbf{k}} - \omega_{\mathbf{k}+(\mathbf{q}-\mathbf{q}_1)}} \right]. \quad (3.19)$$

Apart from the obvious interest in having $\text{Im}M_{q,q_1}$ represented in terms of a sum over hole and particle states, the representation of Eq. (3.17) happens to be most useful in order to define the retarded counterpart of the triple vertex (see the Appendix) and to compare, therefore, analytical representations of the nonlinear stopping power where both retarded and time-ordered response functions are involved. Analytical integration of Eq. (3.19) gives

$$H_{q,q_1} = \text{sgn}(q^0) [f_{q,q_1} - f_{-q,-(q-q_1)}], \quad (3.20)$$

where

Three-point functions M_{q,q_1} and $M_{q,q-q_1}$, represented diagrammatically by empty triangle diagrams with their lines running in opposite directions, give the same contribution to the matrix element of Eq. (2.10). However, it is useful to define the symmetrized functions²⁸

$$M_{q,q_1}^s = \frac{1}{2}(M_{q,q_1} + M_{q,q-q_1}), \quad (3.22)$$

which is invariant under the change $q^0 \rightarrow -q^0$, $q_1^0 \rightarrow$

$-q_1^0$, and

$$H_{q,q_1}^s = \frac{1}{2}(H_{q,q_1} + H_{q,q-q_1}), \quad (3.23)$$

which is an even function of the frequency component of q , q^0 .

In the low-frequency limit, the symmetrized three-point function gives

$$\begin{aligned} M_{\mathbf{q},0;\mathbf{q}_1,0}^s = & -\frac{2q_R^2 m_e^2 \hbar^{-2}}{\pi^2 |\mathbf{q}| |\mathbf{q}_1| |\mathbf{q} - \mathbf{q}_1|} \left\{ \sum_{i=1}^3 \cos \phi_{\mathbf{q}_i} \ln \left| \frac{|\mathbf{q}_i| + 2q_F}{|\mathbf{q}_i| - 2q_F} \right| \right. \\ & - \sqrt{1 - q_F^2/q_R^2} \sum_{i=1}^3 \ln \left| \frac{|\mathbf{q}_j| |\mathbf{q}_k| - 4q_F^2 \cos \phi_{\mathbf{q}_i} + 2|\mathbf{q}_i| q_F \sqrt{1 - q_F^2/q_R^2}}{\sqrt{(4q_F^2 - |\mathbf{q}_j|^2)(4q_F^2 - |\mathbf{q}_k|^2)}} \right| \theta(q_R - q_F) \\ & \left. + \sqrt{q_F^2/q_R^2 - 1} \left[\sum_{i=1}^3 \arccos \frac{|\mathbf{q}_j| |\mathbf{q}_k| - 4q_F^2 \cos \phi_{\mathbf{q}_i}}{\sqrt{(4q_F^2 - |\mathbf{q}_j|^2)(4q_F^2 - |\mathbf{q}_k|^2)}} - 2\pi \right] \theta(q_F - q_R) \right\}, \end{aligned} \quad (3.24)$$

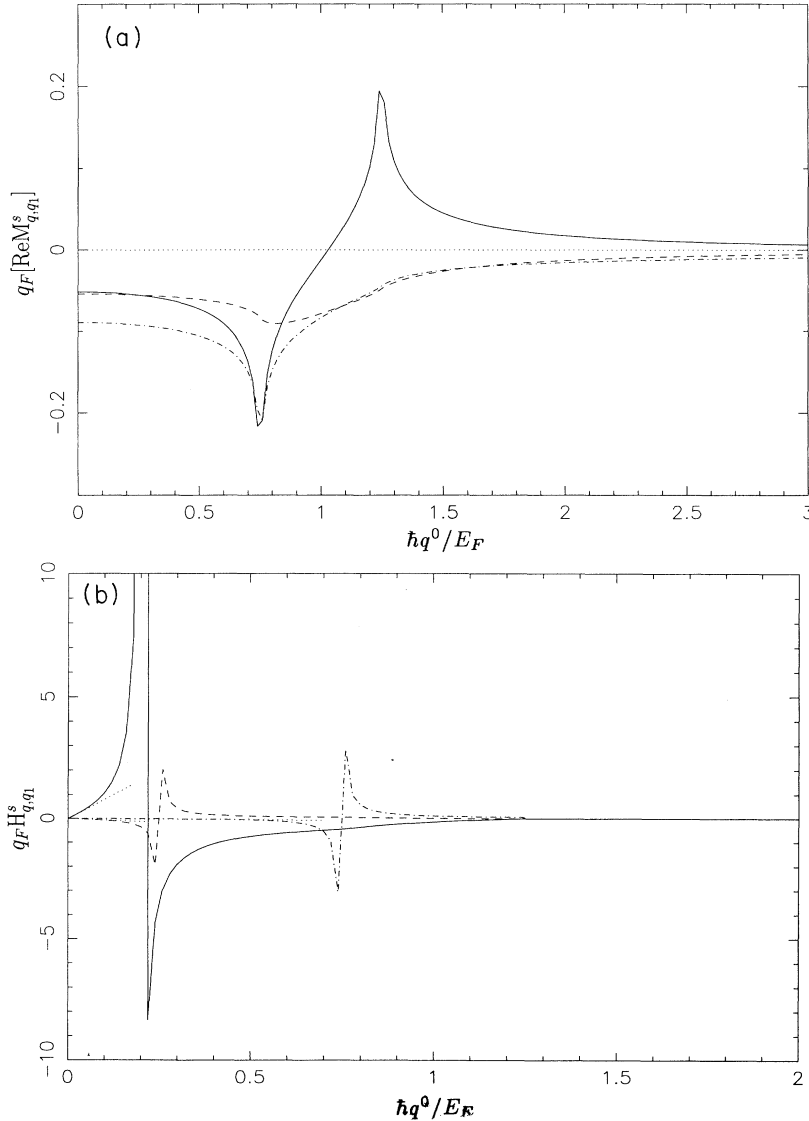


FIG. 5. Universal functions, $q_F [\text{Re} M_{q,q_1}^s]$ (a) and $q_F H_{q,q_1}^s$ (b), as a function of $\hbar q^0 / E_F$, E_F being the Fermi energy, for $q_1^0 = 0$, $\chi = 0$, $|\mathbf{q}| = q_F/2$, and three representative values of $|\mathbf{q}_1|$. In (a), $|\mathbf{q}_1| = 0$ (solid line), $|\mathbf{q}_1| = q_F$ (dashed line), and $|\mathbf{q}_1| = 2q_F$ (dashed-dotted line). In (b), $|\mathbf{q}_1| = 0.1q_F$ (solid line), $|\mathbf{q}_1| = q_F$ (dashed line), and $|\mathbf{q}_1| = 2q_F$ (dashed-dotted line). Dotted lines in (b) represent the low-frequency limit of $q_F H_{q,q_1}^s$, obtained from Eq. (3.27).

which coincides with the retarded quadratic density response function evaluated by Lloyd and Sholl in the low-frequency limit.²⁹ \mathbf{q}_i , \mathbf{q}_j , and \mathbf{q}_k ($i \neq j \neq k$) denote \mathbf{q} , \mathbf{q}_1 , and $\mathbf{q} - \mathbf{q}_1$, q_R is the radius of the circle circumscribing the triangle formed by these vectors, and $\phi_{\mathbf{q}_i}$ represents the angle facing \mathbf{q}_i in this triangle.

In particular, if \mathbf{q} and \mathbf{q}_1 are parallel, $M_{\mathbf{q},0;\mathbf{q}_1,0}^s$ is obtained in terms of the linear density response function of the noninteracting electron gas, $\chi_{\mathbf{q},0}^0$:

$$M_{\mathbf{q},0;\mathbf{q}_1,0}^s = -\frac{2m_e}{|\mathbf{q}||\mathbf{q}_1||\mathbf{q} - \mathbf{q}_1|} \left[|\mathbf{q}_i| \text{Re} \chi_{\mathbf{q}_i,0}^0 - |\mathbf{q}_j| \text{Re} \chi_{\mathbf{q}_j,0}^0 - |\mathbf{q}_k| \text{Re} \chi_{\mathbf{q}_k,0}^0 \right], \quad (3.25)$$

where

$$\mathbf{q}_i = \max(\mathbf{q}, \mathbf{q}_1, \mathbf{q} - \mathbf{q}_1). \quad (3.26)$$

On the other hand, an expansion of the symmetrized function of Eq. (3.23) in powers of the frequency gives, after retaining only the first-order terms,

$$H_{q,q_1}^s \approx -\frac{m_e^3 \hbar^{-3}}{\pi |\mathbf{q}||\mathbf{q}_1||\mathbf{q} - \mathbf{q}_1|} (1 - q_F^2/q_R^2)^{-1/2} \times \text{sgn}(\cos \phi_{\mathbf{q}}) |q^0| \theta(q_R - q_F) \theta(2q_F - |\mathbf{q}|). \quad (3.27)$$

In Figs. 5–7, we give plots of universal functions, $q_F [\text{Re} M_{q,q_1}^s]$ and $q_F H_{q,q_1}^s$, as a function of $\hbar q^0/E_F$, E_F being the Fermi energy, for $q_1^0 = 0$, $\chi = 0$, three repre-

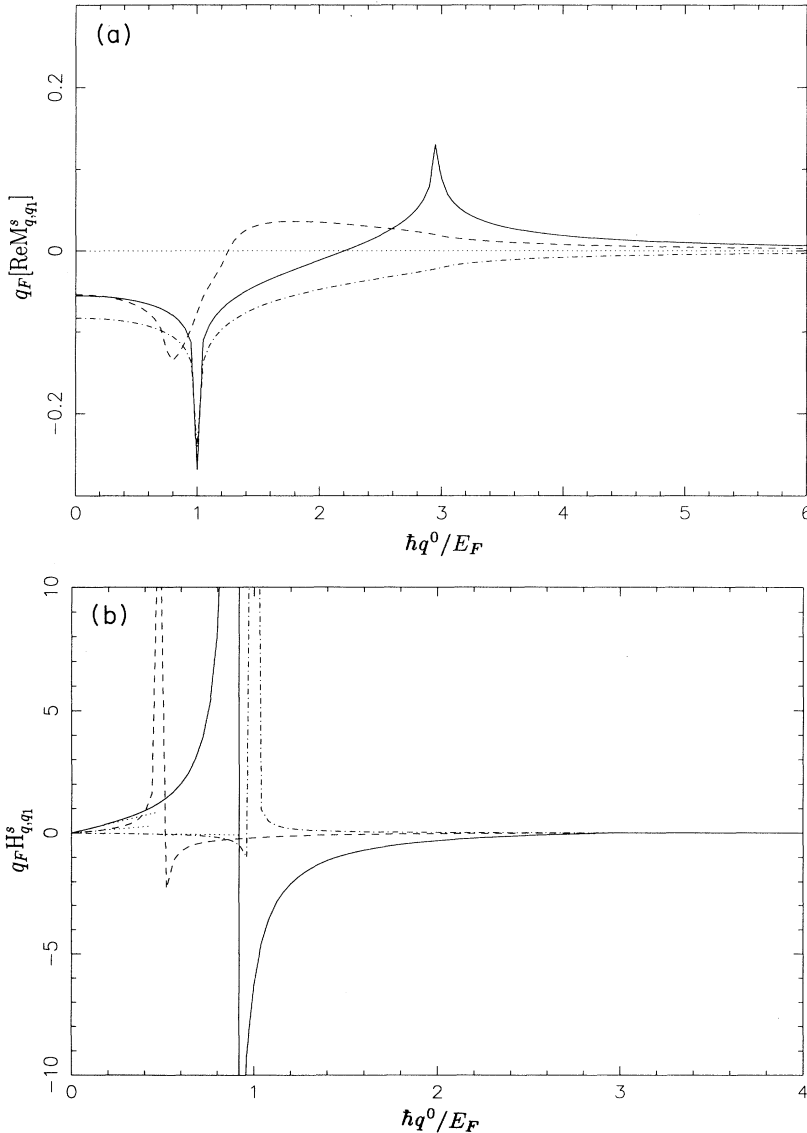


FIG. 6. As in Fig. 5, for $q_1^0 = 0$, $\chi = 0$, $|\mathbf{q}| = q_F$, and three representative values of $|\mathbf{q}_1|$. In (a), $|\mathbf{q}_1| = 0$ (solid line), $|\mathbf{q}_1| = 0.5 q_F$ (dashed line), and $|\mathbf{q}_1| = 2 q_F$ (dashed-dotted line). In (b), $|\mathbf{q}_1| = 0.1 q_F$ (solid line), $|\mathbf{q}_1| = 0.5 q_F$ (dashed line), and $|\mathbf{q}_1| = 2 q_F$ (dashed-dotted line).

representative values of $|\mathbf{q}|$: $|\mathbf{q}| = q_F/2$ (Fig. 5), $|\mathbf{q}| = q_F$ (Fig. 6), and $|\mathbf{q}| = 2q_F$ (Fig. 7), and different values of $|\mathbf{q}_1|$. The dotted lines in Figs. 5(b), 6(b), and 7(b) represent the low-frequency limit of H_{q,q_1}^s , as obtained from Eq. (3.27), showing that it depends linearly on the frequency in a small range of low frequencies, much smaller than the frequency range in which the imaginary part of the linear density response function of the noninteracting electron gas, $\text{Im}\chi_q^0$, is linear. The real part of the symmetrized three-point function, $\text{Re}M_{q,q_1}^s$, happens to be almost constant in the low-frequency limit, and it goes to zero as the frequency goes to infinity. Similar results are obtained for different values of the angle between \mathbf{q} and \mathbf{q}_1 .

IV. SECOND-ORDER STOPPING POWER

The transition rate, γ_q^{single} , for transferring four-momentum q to a free-electron gas by moving a particle from inside the Fermi sea ($|\mathbf{s}| < q_F$) to outside ($|\mathbf{p}| > q_F$), thus creating an electron-hole pair, is derived from the square of the matrix element S_{fi} of Eq. (2.10), represented diagrammatically in Fig. 1

$$\gamma_q^{\text{single}} = 2 \lim_{t \rightarrow \infty} \sum_{\mathbf{s}} n_{\mathbf{s}} \sum_{\mathbf{p}} (1 - n_{\mathbf{p}}) \frac{|S_{fi}|^2}{t} \delta_{q,p-s}^4, \quad (4.1)$$

where $\delta_{q,q'}^4$ is the symmetric Kronecker δ symbol that

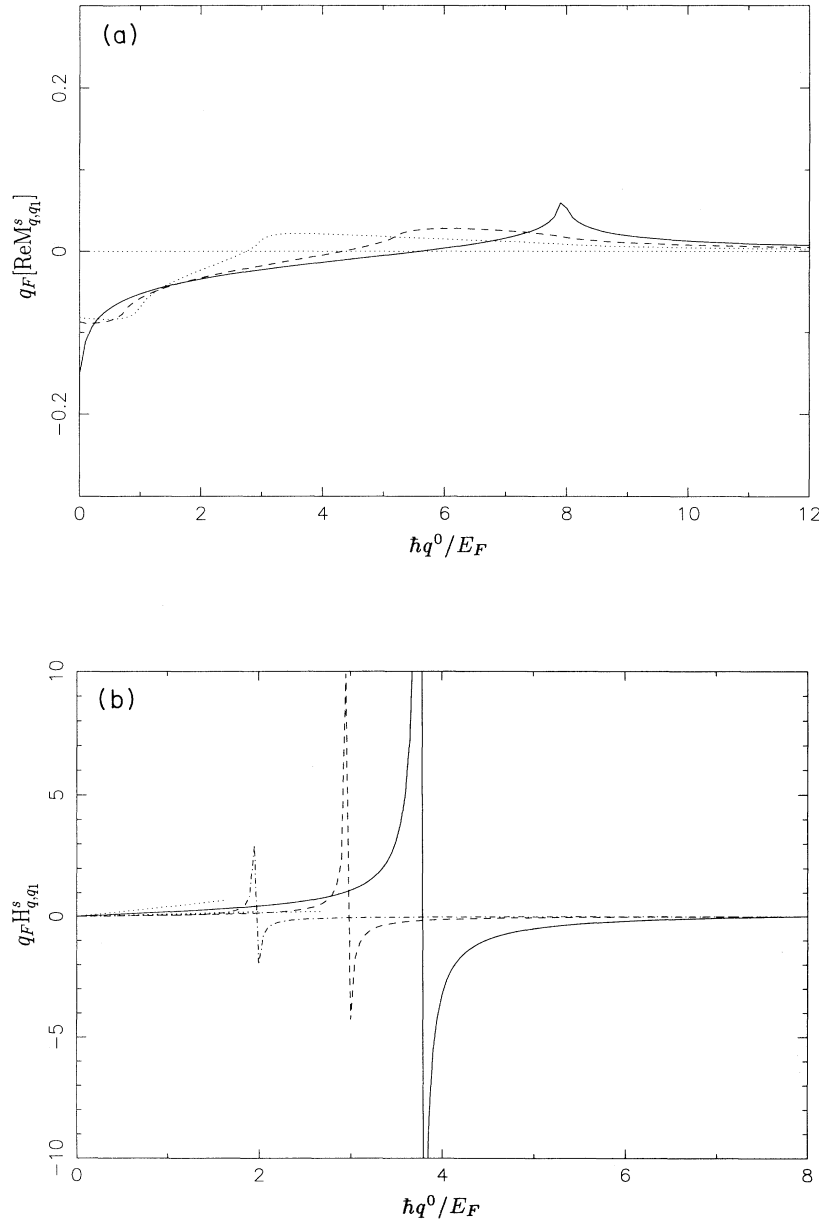


FIG. 7. As in Fig. 5, for $q_1^0 = 0$, $\chi = 0$, $|\mathbf{q}| = 2q_F$, and three representative values of $|\mathbf{q}_1|$. In (a), $|\mathbf{q}_1| = 0$ (solid line), $|\mathbf{q}_1| = 0.5q_F$ (dashed line), and $|\mathbf{q}_1| = q_F$ (dashed-dotted line). In (b), $|\mathbf{q}_1| = 0.1q_F$ (solid line), $|\mathbf{q}_1| = 0.5q_F$ (dashed line), and $|\mathbf{q}_1| = q_F$ (dashed-dotted line).

equals unity if $q = q'$ and is zero otherwise, and t represents the interaction time.

Within the RPA, $g_1(s, p) = g_2(s, p, q_1) = 0$ in Eq. (2.10), and the square of the matrix element corresponding to single excitations gives, therefore, up to third order in the ion charge

$$|S_{fi}|^2 = B_q + \int \frac{d^4 q_1}{(2\pi)^4} \text{Re} [C_{q, q_1} G_{s+q_1}^0], \quad (4.2)$$

where B_q gives the contribution coming from the creation of an electron-hole pair through one-step interactions, and is represented by the square of the first diagram and the cross product between the first and third diagrams of Fig. 1:

$$B_q = \frac{2\pi\hbar^{-2}}{\Omega^2} t Z_1^2 v_{\mathbf{q}}^2 |\epsilon_{\mathbf{q}}|^{-2} \delta(q^0 - \mathbf{q} \cdot \mathbf{v}) \times \left[1 + 4\pi\hbar^{-2} Z_1 \int \frac{d^4 q_1}{(2\pi)^4} v_{\mathbf{q}_1} v_{\mathbf{q}-\mathbf{q}_1} \times \text{Re} [\epsilon_{q_1}^{-1} \epsilon_{q-q_1}^{-1} M_{q, q_1}^s] \delta(q_1^0 - \mathbf{q}_1 \cdot \mathbf{v}) \right]. \quad (4.3)$$

This contribution to the absorption probability of Eq. (4.1) depends, within the RPA, on \mathbf{s} and \mathbf{p} only through $q = p - s$, and is easily shown to be proportional to $\text{Im}\chi_{\mathbf{q}}^0$. The second term of Eq. (4.2) gives the contribution coming from the creation of an electron-hole pair through two-step interactions, represented by the cross product between the first and second diagrams of Fig. 1, it depends, therefore, on \mathbf{s} or \mathbf{p} separately through $G_{s+q_1}^0$, and

$$C_{q, q_1} = -\frac{4\pi\hbar^{-3}}{\Omega^2} t Z_1^3 v_{\mathbf{q}} v_{\mathbf{q}_1} v_{\mathbf{q}-\mathbf{q}_1} (\epsilon_{\mathbf{q}}^{-1})^* \epsilon_{\mathbf{q}_1}^{-1} \epsilon_{\mathbf{q}-\mathbf{q}_1}^{-1} \times \delta(q^0 - \mathbf{q} \cdot \mathbf{v}) \delta(q_1^0 - \mathbf{q}_1 \cdot \mathbf{v}). \quad (4.4)$$

Then, by summing the square of the matrix element over initial and final states and using the representations of Eqs. (3.8) and (3.18), we find

$$\gamma_q^{\text{single}} = -\frac{4\pi\hbar^{-1}}{\Omega} Z_1^2 v_{\mathbf{q}} \delta(q^0 - \mathbf{q} \cdot \mathbf{v}) \theta(q^0) \lim_{t \rightarrow \infty} \frac{1}{t} \times \left\{ \text{Im}\epsilon_{\mathbf{q}}^{-1} \left[1 + 4\pi\hbar^{-2} Z_1 \int \frac{d^4 q_1}{(2\pi)^4} v_{\mathbf{q}_1} v_{\mathbf{q}-\mathbf{q}_1} \text{Re} [\epsilon_{q_1}^{-1} \epsilon_{q-q_1}^{-1} M_{q, q_1}^s] \delta(q_1^0 - \mathbf{q}_1 \cdot \mathbf{v}) \right] + 4\pi\hbar^{-2} Z_1 \int \frac{d^4 q_1}{(2\pi)^4} v_{\mathbf{q}_1} v_{\mathbf{q}-\mathbf{q}_1} \text{Re} [(\epsilon_{\mathbf{q}}^{-1})^* \epsilon_{\mathbf{q}_1}^{-1} \epsilon_{\mathbf{q}-\mathbf{q}_1}^{-1} (H_{q, q_1} + iJ_{q, q_1})] \delta(q_1^0 - \mathbf{q}_1 \cdot \mathbf{v}) \right\}, \quad (4.5)$$

where

$$J_{q, q_1} = (2\pi)^4 \int \frac{d^3 s}{(2\pi)^3} n_{\mathbf{s}} \int \frac{d^3 p}{(2\pi)^3} (1 - n_{\mathbf{p}}) \delta^4(q - p + s) \text{Im} G_{s+q_1}. \quad (4.6)$$

The transition rate γ_q^{double} for transferring four-momentum q to a free-electron gas by creating a double excitation, i.e., by moving two particles from inside the Fermi sea ($|\mathbf{s}_1| < q_F$ and $|\mathbf{s}_2| < q_F$) to outside ($|\mathbf{p}_1| > q_F$ and $|\mathbf{p}_2| > q_F$), is derived from the square of the matrix element $S_{f_1 f_2, i_1 i_2}$ of Eq. (2.18):

$$\gamma_q^{\text{double}} = 4 \lim_{t \rightarrow \infty} \sum_{\mathbf{q}_1} \sum_{\mathbf{s}_1} n_{\mathbf{s}_1} \sum_{\mathbf{s}_2} n_{\mathbf{s}_2} \sum_{\mathbf{p}_1} (1 - n_{\mathbf{p}_1}) \sum_{\mathbf{p}_2} (1 - n_{\mathbf{p}_2}) \frac{|S_{f_1 f_2, i_1 i_2}|^2}{t} \delta_{q_1, p_1 - s_1}^4 \delta_{q - q_1, p_2 - s_2}^4. \quad (4.7)$$

Neglecting all kind of vertex and self-energy insertions, as well as vertex ladder contributions, this matrix element can be represented diagrammatically, up to second order in the ion charge, as in Fig. 8. Contributions to the square of this matrix element that are proportional to Z_1^2 are of higher order in the effective interaction than RPA Z_1^2 contributions to $|S_{fi}|^2$, and they are neglected, therefore, within this approximation. However, contributions that are proportional to Z_1^3 are of the same order as the

Z_1^3 contributions of Eq. (4.2), and they need, therefore, to be taken into account:

$$|S_{f_1 f_2, i_1 i_2}|^2 = D_{q, q_1} + \text{Re} [E_{q, q_1} G_{s+q_1}^0], \quad (4.8)$$

where D_{q, q_1} gives the contribution coming from the creation of two real excitations through one-step interactions, represented by the cross product between the second and third diagrams of Fig. 8, and depends on $(\mathbf{s}_1, \mathbf{p}_1)$

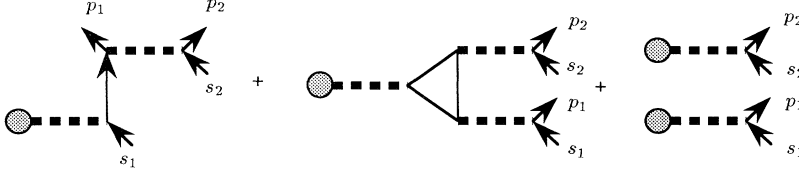


FIG. 8. Diagrammatic representation, up to second order in the ion charge, of the RPA matrix element of Eq. (2.18), where all vertex and self-energy insertions have been neglected, as well as vertex ladder contributions.

and (s_2, p_2) only through $q_1 = p_1 - s_1$ and $q - q_1 = p_2 - s_2$:

$$D_{q,q_1} = -\frac{8\pi^2\hbar^{-5}}{\Omega^4} t Z_1^3 v_{\mathbf{q}} v_{\mathbf{q}_1}^2 v_{\mathbf{q}-\mathbf{q}_1}^2 |\epsilon_{q_1}|^{-2} |\epsilon_{q-q_1}|^{-2} \times \text{Im}[\epsilon_q^{-1} M_{q,q_1}^s] \delta(q^0 - \mathbf{q} \cdot \mathbf{v}) \delta(q_1^0 - \mathbf{q}_1 \cdot \mathbf{v}), \quad (4.9)$$

and E_{q,q_1} gives the contribution coming from the creation of two real excitations through one- and two-step interactions, represented by the cross product between the first

and third diagrams of Fig. 8:

$$E_{q,q_1} = -i \frac{8\pi^2\hbar^{-4}}{\Omega^4} t Z_1^3 v_{\mathbf{q}} v_{\mathbf{q}_1} v_{\mathbf{q}-\mathbf{q}_1}^2 \epsilon_q^{-1} (\epsilon_{q_1}^{-1})^* |\epsilon_{q-q_1}^{-1}|^2 \times \delta(q^0 - \mathbf{q} \cdot \mathbf{v}) \delta(q_1^0 - \mathbf{q}_1 \cdot \mathbf{v}). \quad (4.10)$$

Then, by summing the square of the matrix element of Eq. (4.8) over initial and final states and using again the representations of Eqs. (3.8) and (3.18), we find

$$\begin{aligned} \gamma_q^{\text{double}} &= \frac{4\pi\hbar^{-1}}{\Omega^2} \delta(q^0 - \mathbf{q} \cdot \mathbf{v}) \lim_{t \rightarrow \infty} \frac{1}{t^2} \\ &\times \sum_{q_1} \theta(q_1^0) \theta(q^0 - q_1^0) \left\{ -4\pi\hbar^{-2} \text{Im} \epsilon_{q_1}^{-1} \text{Im} \epsilon_{q-q_1}^{-1} Z_1 v_{\mathbf{q}_1} v_{\mathbf{q}-\mathbf{q}_1} \text{Im} [\epsilon_q^{-1} M_{q,q_1}^s] \right. \\ &\left. - 8\pi\hbar^{-2} Z_1 v_{\mathbf{q}_1} v_{\mathbf{q}-\mathbf{q}_1} \text{Im} [\epsilon_q^{-1} (\epsilon_{q_1}^{-1})^* \epsilon_{q-q_1}^{-1} (H_{q_1,q} + iJ_{q_1,q})] \right\} \delta(q_1^0 - \mathbf{q}_1 \cdot \mathbf{v}). \end{aligned} \quad (4.11)$$

Finally, the stopping power is obtained as the energy loss per unit path length of the projectile, after multiplying the inverse mean free path γ_q/v by the energy transfer $\hbar q^0$ and summing over q :

$$-\frac{dE}{dx} = \frac{1}{v} \sum_q \hbar q^0 (\gamma_q^{\text{single}} + \gamma_q^{\text{double}}), \quad (4.12)$$

and introduction of Eqs. (4.5) and (4.11) into Eq. (4.12) gives, after some algebra, the following result:

$$\begin{aligned} -\frac{dE}{dx} &= -2 \frac{Z_1^2}{v} \int \frac{d^3q}{(2\pi)^3} \omega v_{\mathbf{q}} \text{Im} \epsilon_{\mathbf{q},\omega}^{-1} \theta(\omega) \\ &- 4 \frac{Z_1^3}{v\hbar^2} \int \frac{d^3q}{(2\pi)^3} \omega v_{\mathbf{q}} \int \frac{d^3q_1}{(2\pi)^3} v_{\mathbf{q}_1} v_{\mathbf{q}-\mathbf{q}_1} \\ &\times [f_1(\mathbf{q}, \omega, \mathbf{q}_1, \omega_1) + f_2(\mathbf{q}, \omega, \mathbf{q}_1, \omega_1) \\ &+ f_3(\mathbf{q}, \omega, \mathbf{q}_1, \omega_1)] \theta(\omega), \end{aligned} \quad (4.13)$$

where

$$f_1(q, q_1) = \text{Im} \epsilon_q^{-1} \text{Re} \epsilon_{q_1}^{-1} \text{Re} \epsilon_{q-q_1}^{-1} \text{Re} M_{q,q_1}^s, \quad (4.14)$$

$$f_2(q, q_1) = \text{Re} \epsilon_q^{-1} \text{Re} \epsilon_{q_1}^{-1} \text{Re} \epsilon_{q-q_1}^{-1} H_{q,q_1}^s, \quad (4.15)$$

and

$$f_3(q, q_1) = -2 \text{Im} \epsilon_q^{-1} \text{Im} \epsilon_{q_1}^{-1} \text{Re} \epsilon_{q-q_1}^{-1} H_{q_1,q}^s, \quad (4.16)$$

with

$$\omega = \mathbf{q} \cdot \mathbf{v} \quad (4.17)$$

and

$$\omega_1 = \mathbf{q}_1 \cdot \mathbf{v}. \quad (4.18)$$

The contribution to the stopping power of Eq. (4.13) that is proportional to Z_1^2 exactly coincides with the standard well-known result,³⁰ which in the high-velocity limit approaches the formula of Bethe.

The Z_1^3 contribution to the stopping power has been split into three terms. The first one comes from B_q of Eq. (4.3), i.e., from the cross product between the first and third diagrams of Fig. 1, and gives, therefore, the contribution from losses to one-step excitations generated by the quadratically screened ion potential, while the second term comes from C_{q,q_1} of Eq. (4.4), i.e., from the cross product between the first and second diagrams of Fig. 1, and gives the contribution from losses to two-step excitations generated by the linearly screened ion potential. The third term comes from both B_q and C_{q,q_1} , and from losses to double excitations, too. Also, we find that there is no contribution to the Z_1^3 stopping power that is proportional to the product of three imaginary parts of the dielectric function, as a result of a cancellation between contributions from C_{q,q_1} and E_{q,q_1} , representing losses to single and double excitations, respectively.

It is well known that the stopping power of an electron gas can, also, be obtained from the induced retarding force that the polarization charge distribution in the

vicinity of the projectile exerts on the projectile itself, and it is found, therefore, to be given by the following expression:³⁰

$$S = \frac{Z_1 e}{v} \nabla \phi(\mathbf{r}, t)|_{\mathbf{r}=\mathbf{v}t \cdot \mathbf{v}}, \quad (4.19)$$

where $\phi(\mathbf{r}, t)$ represents the so-called wake potential, that is, the potential induced by the projectile in the medium.

The wake potential can be calculated as the mean value of the interaction between a test unit positive charge at

\mathbf{r} and the electron gas

$$\phi(\mathbf{r}, t) = \frac{\langle \Psi_0 | V_H(\mathbf{r}, t) | \Psi_0 \rangle}{\langle \Psi_0 | \Psi_0 \rangle}, \quad (4.20)$$

where $|\Psi_0\rangle$ is the Heisenberg ground state of the interacting system and $V_H(\mathbf{r}, t)$ represents the potential of the interaction between a test positive unit charge at \mathbf{r} and the electron gas, in the Heisenberg picture, and one finds, up to second order in the ion charge:³¹

$$\begin{aligned} \phi(\mathbf{r}, t) = & Z_1 e^{-1} \int \frac{d^3 q}{(2\pi)^3} e^{i(\mathbf{q}\cdot\mathbf{r}-\omega t)} v_{\mathbf{q}} [(\epsilon_{\mathbf{q},\omega}^R)^{-1} - 1] + Z_1^2 e^{-1} \hbar^{-2} \int \frac{d^3 q}{(2\pi)^3} e^{i(\mathbf{q}\cdot\mathbf{r}-\omega t)} v_{\mathbf{q}} \\ & \times \int \frac{d^3 q_1}{(2\pi)^3} v_{\mathbf{q}_1} v_{\mathbf{q}-\mathbf{q}_1} (\epsilon_{\mathbf{q},\omega}^R)^{-1} (\epsilon_{\mathbf{q}_1,\omega_1}^R)^{-1} (\epsilon_{\mathbf{q}-\mathbf{q}_1,\omega-\omega_1}^R)^{-1} M_{\mathbf{q},\omega;\mathbf{q}_1,\omega_1}^R, \end{aligned} \quad (4.21)$$

$\epsilon_{\mathbf{q}}^R$ and $M_{\mathbf{q},\mathbf{q}_1}^R$ representing retarded response functions, as defined in the Appendix. Then, introduction of this potential into Eq. (4.19) gives

$$\begin{aligned} -\frac{dE}{dx} = & -\frac{Z_1^2}{v} \int \frac{d^3 q}{(2\pi)^3} \omega v_{\mathbf{q}} \text{Im}(\epsilon_{\mathbf{q},\omega}^R)^{-1} \\ & -\frac{Z_1^3}{v\hbar^2} \int \frac{d^3 q}{(2\pi)^3} \omega v_{\mathbf{q}} \int \frac{d^3 q_1}{(2\pi)^3} v_{\mathbf{q}_1} v_{\mathbf{q}-\mathbf{q}_1} \text{Im} [(\epsilon_{\mathbf{q},\omega}^R)^{-1} (\epsilon_{\mathbf{q}_1,\omega_1}^R)^{-1} (\epsilon_{\mathbf{q}-\mathbf{q}_1,\omega-\omega_1}^R)^{-1} M_{\mathbf{q},\omega;\mathbf{q}_1,\omega_1}^R]. \end{aligned} \quad (4.22)$$

This expression for the stopping power, which is equivalent³² to the result obtained in Refs. 13, 14, and 16, is shown in the Appendix to be equivalent to Eq. (4.13) above.

A. Low-velocity limit

Due to the fact that $\omega = \mathbf{q} \cdot \mathbf{v}$ and $\omega_1 = \mathbf{q}_1 \cdot \mathbf{v}$ in Eq. (4.13), in the low-velocity limit only the low-frequency forms of the response functions involved enter, thus the

contribution to the stopping power that is proportional to Z_1^2 being, in this limit, proportional to the velocity, as well as contributions to the Z_1^3 stopping power coming from f_1 and f_2 of Eqs. (4.14) and (4.15), while contributions to the Z_1^3 stopping power coming from f_3 of Eq. (4.16) is proportional to v^3 . Hence, if one keeps only the lowest-order terms in the velocity of the projectile, insertion of the low-frequency limits of both linear and quadratic response functions into Eq. (4.13) gives the following result for the low-velocity limit of the stopping power, up to third order in the ion charge:

$$-\frac{dE}{dx} = \frac{4}{3\pi} Z_1^2 \frac{m e^4}{\hbar^2} a_0^{-1} (v/v_0) \int \frac{dq}{q} (\epsilon_{\mathbf{q},0})^{-2} + \frac{16}{3\pi m_e} Z_1^3 (v/v_0) \int_0^\infty dq q^2 \int_0^\infty dq_1 \int_{-1}^1 d\chi \frac{f_1^L + f_2^L}{|\mathbf{q} - \mathbf{q}_1|^2}, \quad (4.23)$$

where

$$f_1^L = A_{\mathbf{q}} \epsilon_{\mathbf{q},0}^{-2} \epsilon_{\mathbf{q}_1,0}^{-1} \epsilon_{\mathbf{q}-\mathbf{q}_1,0}^{-1} M_{\mathbf{q},0;\mathbf{q}_1,0}^s, \quad (4.24)$$

and

$$f_2^L = B_{\mathbf{q},\mathbf{q}_1} \epsilon_{\mathbf{q},0}^{-1} \epsilon_{\mathbf{q}_1,0}^{-1} \epsilon_{\mathbf{q}-\mathbf{q}_1,0}^{-1}, \quad (4.25)$$

with

$$A_{\mathbf{q}} = \frac{2}{(qa_0)^3} \theta(2q_F - q) \quad (4.26)$$

and

$$\begin{aligned} B_{\mathbf{q},\mathbf{q}_1} = & -\frac{m_e}{\pi q q_1 |\mathbf{q} - \mathbf{q}_1| a_0^3} (1 - q_F^2/q_R^2)^{-1/2} \\ & \times \text{sgn}(\cos \phi_{\mathbf{q}}) \theta(2q_F - q) \theta(q_R - q_F), \end{aligned} \quad (4.27)$$

a_0 and v_0 being the radius and the velocity of Bohr, $a_0 =$

\hbar^2/m_e^2 and $v_0 = e^2/\hbar$, respectively.

From the Z_1^2 contribution to the stopping power of Eq. (4.23), the low-velocity limit of Lindhard and Winther³³ can be derived, after expanding $\epsilon_{\mathbf{q},0}$ in powers of q/q_F , and in the limit of high densities ($v_F \gg v_0$) the formula of Fermi and Teller³⁴ is obtained. These formulas can, also, be obtained on the basis of the free-electron picture, with the additional assumption of independent, individual, elastic electron scattering. In this case, the average energy loss per unit path length for an arbitrary ion moving with velocity \mathbf{v} through an electron gas of a constant density n is given, in the low-velocity limit, by

$$-\frac{dE}{dx} = nm_e v_F \sigma_{tr}(v_F)v, \quad (4.28)$$

where

$$\sigma_{tr}(w) = \frac{\pi}{(mw/\hbar)^4} \int_0^{2mw/\hbar} dq q^3 |f(q)|^2 \quad (4.29)$$

is the so-called transport cross section, $f(q)$ representing the scattering amplitude for transferring momentum \mathbf{q} . Since $f(q)$ is obtained in terms of the screened potential of the ion, once the dielectric function of the medium is given, the stopping power can be evaluated, within linear response theory, from Eq. (4.28), and both the formula of Lindhard and Winther and the formula obtained by Fermi and Teller can be derived in this way.

Nagy and Echenique³⁵ have gone further to employ the second Born approximation for the scattering amplitude, characterizing the screening of the projectile in the electron gas by a Yukawa potential, and have derived a Z_1^3 correction to the formula of Fermi and Teller, which is, in the high density limit, in good agreement with the Z_1^3

contribution to Eq. (4.23). The Z_1^3 contribution to Eq. (4.23) is, also, exactly equivalent to the result derived in the low-velocity limit by Hu and Zaremba.¹⁴

Echenique *et al.*³⁶ extended this method and evaluated the nonlinear stopping power of an electron gas for slow ions, from Eq. (4.28), by using the density-functional formulation of Hohenberg and Kohn, and Kohn and Sham³⁷ to calculate the exact scattering amplitude on the basis of the self-consistent potential generated by a static charge submerged in an electron gas, and were able, therefore, to evaluate, within the low-velocity limit, the stopping power to all orders in Z_1 .

B. High-velocity limit

For high velocities, the zero-point motion of the electron gas can be neglected and it can be considered, therefore, as if it were at rest. Thus, in this approximation all \mathbf{k} , the momenta of the electrons, become equal to zero, and Eq. (3.6) leads to the well-known static electron gas approximation for the dielectric function

$$\epsilon_q = 1 - \frac{\omega_p^2}{\omega^2 - \omega_q^2}, \quad (4.30)$$

where

$$\omega_p = \sqrt{4\pi n e^2 / m_e} \quad (4.31)$$

represents the plasma frequency of the electron gas, and

$$\omega = q^0 + i\eta_q. \quad (4.32)$$

Similarly, one can set all \mathbf{k} equal to zero in Eq. (3.10) to obtain

$$\begin{aligned} M_{q,q_1}^s = & -n \{ \omega_1(\omega - \omega_1)\omega_q^2 - \omega(\omega - \omega_1)\omega_{q_1}^2 - \omega\omega_1\omega_{q-q_1}^2 (\omega - \omega_1)\omega_q\omega_{q_1} \\ & + \omega_1^2\omega_q\omega_{q-q_1} + \omega_q^2\omega_{q_1}\omega_{q-q_1} - \omega_q\omega_{q_1}\omega_{q-q_1}(\omega_q + \omega_{q_1} + \omega_{q-q_1}) \} \\ & \times \{ (\omega^2 - \omega_q^2)(\omega_1^2 - \omega_{q_1}^2) [(\omega - \omega_1)^2 - \omega_{q-q_1}^2] \}^{-1}, \end{aligned} \quad (4.33)$$

which exactly coincides, in the low- q limit, with the low- q limit of the full three-point function of Eq. (3.4),³⁸ and

$$\begin{aligned} H_{q,q_1}^s = & \pi n \operatorname{sgn}(q^0) \left\{ \delta(q^0 - \omega_q) \left[\frac{1}{q_1^0 - \omega_{q_1}} \right. \right. \\ & \left. \left. + \frac{1}{-q_1^0 + \omega_q - \omega_{q-q_1}} \right] \right. \\ & \left. - \delta(q^0 + \omega_q) \left[\frac{1}{q_1^0 + \omega_q - \omega_{q-q_1}} + \frac{1}{-q_1^0 - \omega_{q_1}} \right] \right\}. \end{aligned} \quad (4.34)$$

Now, introduction of Eqs. (4.30) and (4.34) into Eqs. (4.15) and (4.16) results in f_2 and f_3 giving no contribution to the integral of Eq. (4.13), and, we can conclude,

therefore, that for the electron gas at rest only the real part of the three-point function contributes to the Z_1^3 effect. Then, after substitution of the static electron gas approximations to both the linear and quadratic response functions, ϵ_q and M_{q,q_1} , into Eq. (4.14), and Eq. (4.14) into Eq. (4.13), one finds

$$-\frac{dE}{dx} = \frac{4\pi n Z_1^2 e^4}{m_e v^2} (L_0 + Z_1 L_1), \quad (4.35)$$

where

$$L_0 = \ln \frac{q_{\max}}{q_{\min}}, \quad (4.36)$$

and L_1 is the Z_1^3 correction to the stopping number, which coincides with the result obtained in this approximation in Refs. 12 and 16:

$$L_1 = \frac{1}{\pi^2 a_0} \int_{q_{\min}}^{q_{\max}} \frac{dq}{q} \times \int d\mathbf{q}_1 \frac{Q_{q, \mathbf{q}_1}}{q_1^2 |\mathbf{q} - \mathbf{q}_1|^2 [\omega_1 - \alpha_{\mathbf{q}_1}^2] [(\omega - \omega_1)^2 - \alpha_{\mathbf{q} - \mathbf{q}_1}^2]}, \quad (4.37)$$

with

$$q_{\min} = \left\{ \frac{2m^2 v^2}{\hbar^2} \left[1 - \sqrt{1 - (\hbar\omega_p/mv^2)^2} \right] \right\}^{1/2}, \quad (4.38)$$

$$q_{\max} = \left\{ \frac{2m^2 v^2}{\hbar^2} \left[1 + \sqrt{1 - (\hbar\omega_p/mv^2)^2} \right] \right\}^{1/2}, \quad (4.39)$$

$$\alpha_{\mathbf{q}} = \sqrt{\omega_p^2 + \omega_{\mathbf{q}}^2}, \quad (4.40)$$

and

$$Q_{q, \mathbf{q}_1} = -\left\{ \omega_1(\omega - \omega_1)\omega_{\mathbf{q}}^2 - \omega(\omega - \omega_1)\omega_{\mathbf{q}_1}^2 - \omega\omega_1\omega_{\mathbf{q} - \mathbf{q}_1}^2 + (\omega - \omega_1)\omega_{\mathbf{q}}\omega_{\mathbf{q}_1} + \omega_1^2\omega_{\mathbf{q}}\omega_{\mathbf{q} - \mathbf{q}_1} + \omega^2\omega_{\mathbf{q}_1}\omega_{\mathbf{q} - \mathbf{q}_1} - \omega_{\mathbf{q}}\omega_{\mathbf{q}_1}\omega_{\mathbf{q} - \mathbf{q}_1}(\omega_{\mathbf{q}} + \omega_{\mathbf{q}_1} + \omega_{\mathbf{q} - \mathbf{q}_1}) \right\}. \quad (4.41)$$

In particular, in the limit as $mv^2 \gg \hbar\omega_p$, L_0 is very easily found to be given by

$$L_0 \approx \ln \frac{2mv^2}{\hbar\omega_p}, \quad (4.42)$$

which gives the formula of Bethe for the Z_1^2 contribution to the stopping power. On the other hand, as far as the Z_1^3 correction to the stopping number, L_1 , is concerned, one can approximate, in the classical limit

$$\alpha_{\mathbf{q}} = \omega_p, \quad (4.43)$$

the lower q limit being, therefore,

$$q_{\min} = \frac{\omega_p}{v} \quad (4.44)$$

and choosing the upper limit q_{\max} to be the maximum momentum transfer:

$$q_{\max} = \frac{2mv}{\hbar}. \quad (4.45)$$

An analytical evaluation of the integrations involved in Eq. (4.37) gives

$$(L_1)_{\text{classical}} = \frac{5}{3} \frac{\pi\omega_p}{v^3} \left[\ln \frac{2mv^2}{2.13\hbar\omega_p} + O(v^{-4}) \right]. \quad (4.46)$$

Furthermore, numerical study shows that introduction of the full $\alpha_{\mathbf{q}}$ of Eq. (4.40) gives a result for L_1 with the same dependence on v as the classical approximation of Eq. (4.46), though it is smaller than the classical result by an approximate factor of 1.17, so that the full L_1 can be approximated by

$$L_1 \approx 1.42 \frac{\pi\omega_p}{v^3} \ln \frac{2mv^2}{2.13\hbar\omega_p}, \quad (4.47)$$

which is very close to the result obtained by using twice the prediction of Ashley, Ritchie, and Brandt⁸ with the minimum impact parameter equal to the radius of the quantal harmonic oscillator:³⁹

$$(L_1)_{J-M} = \frac{3}{2} \frac{\pi\omega_p}{v^3} \ln \frac{2mv^2}{2.77\hbar\omega_p}. \quad (4.48)$$

Finally, the velocity distribution of the electron gas, which is completely neglected in the static electron gas approximation, can be accounted for approximately by introducing the plasmon-pole approximation to the response functions.⁴⁰ In this approximation the Z_1^3 correction to the stopping power is also given by Eq. (4.35), but now with the plasmon dispersion relation

$$\alpha_{\mathbf{q}}^2 = \omega_p^2 + \beta^2 q^2 + \omega_{\mathbf{q}}^2, \quad (4.49)$$

where

$$\beta^2 = \frac{3}{5} q_F^2 \quad (4.50)$$

represents the so-called mean-square velocity of the electron gas.

V. RESULTS

First of all, we show in Fig. 9 the low-velocity limit of the Z_1^3 contribution to the stopping power, as calculated from Eq. (4.23) and divided by the velocity of the ion, as a function of the electron density parameter r_s . Z_1^3 contributions to the stopping power from f_1^L and f_2^L of Eqs. (4.24) and (4.25), representing losses to single excitations generated by the quadratically screened ion potential and losses from multiply scattered excitations generated by the linearly screened ion potential, respectively, are also plotted separately in the same figure (dashed and dashed-dotted lines), showing that the Z_1^3 term arising from the quadratically screened interaction is negative, although it is positive and the dominant contribution at higher velocities, as will be shown below. This is a consequence of the fact that in the low-velocity limit nonlinear screening of the ion leads to a weaker potential than that found in the linear theory. On the other hand, nonlinear corrections are of increasing importance at lower densities, which is due to the well-known fact that at lower densities the kinetic energy of the electron gas diminishes and the ion potential becomes a relatively stronger perturbation. The Z_1^3 correction accounts, therefore, in the low-velocity limit, for nonlinear corrections only at high electron densities and small ion charges.

The stars in Fig. 9 represent, also in the low-velocity limit, the full nonlinear contribution to the stopping power, multiplied by a factor of -1 , obtained from a density-functional theory (DFT) calculation for antiprotons to all orders in Z_1 ,⁴¹ and coincides, as one expected, with our Z_1^3 correction in the high density limit. The full nonlinear contribution to the stopping power obtained from a DFT calculation for protons, represented by circles in the same figure, also coincides with the Z_1^3 correc-

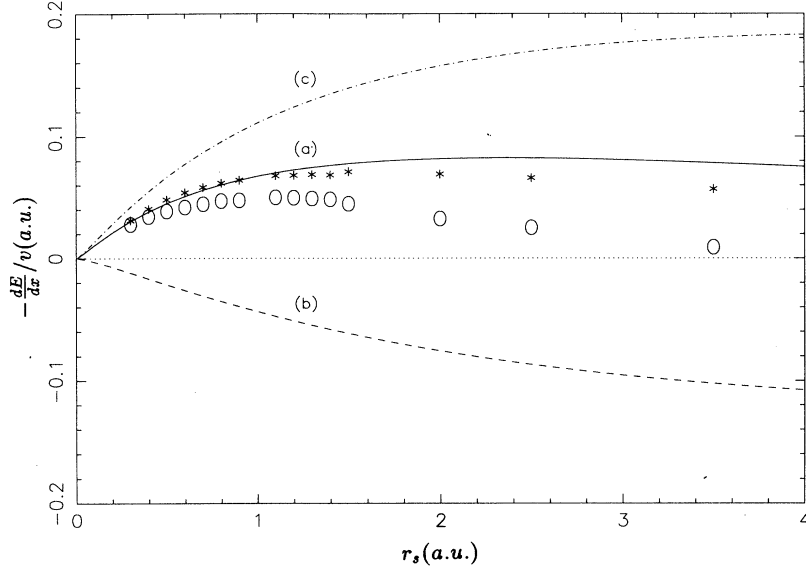


FIG. 9. The contribution to the stopping power of Eq. (4.23), divided by the velocity power of the projectile, that is proportional to Z_1^3 [solid line labeled (a)], as a function of r_s , for $Z_1 = 1$. Z_1^3 contributions from f_1^L and f_2^L of Eqs. (4.24) and (4.25) are plotted separately by lines labeled (b) and (c), respectively. The stars represent the full nonlinear contribution to the stopping power for antiprotons, given in Ref. 41, multiplied by a factor of -1 , and the circles, the full nonlinear contribution to the stopping power for protons. Both the stopping power and r_s are given in atomic units, i.e., $e = \hbar = m_e = 1$.

tion, in the high density limit, although differences are bigger in this case for lower densities, due to the fact that electronic states bound to the proton may appear now.

We have also calculated the Z_1^3 correction to the electronic stopping power for arbitrary velocities of the projectile, after substitution of the full RPA response functions of Eqs. (3.6) and (3.10) into Eq. (4.13). The result of this calculation for an electron density parameter equal to that of aluminum, $r_s = 2.07$, is plotted in Fig. 10 by a solid line labeled (b), as a function of the velocity of the projectile. Contributions from f_1 , f_2 , and f_3 of Eqs. (4.14), (4.15), and (4.16) are also plotted separately by lines labeled (c), (d), and (e), respectively, and the dotted line represents the low-velocity limit from Eq. (4.23). In the same figure we have also plotted, for comparison,

by a solid line labeled (a), the total Z_1^2 contribution to the stopping power, together with the corresponding low-velocity limit (dotted line).

It is interesting to notice from Fig. 10 that the range of validity of the linear velocity dependence of the Z_1^3 correction persists up to velocities approaching the Fermi velocity of the electron gas. This is, however, a consequence of two competing effects. First, there is the effect of single excitations generated by the quadratically screened ion potential, represented by a dashed line, and, then, the effect of multiply scattered excitations generated by the linearly screened ion potential, represented by a dashed-dotted line, which is very small at high velocities of the ion when the velocity distribution of target electrons can be neglected. Indeed, in this case the

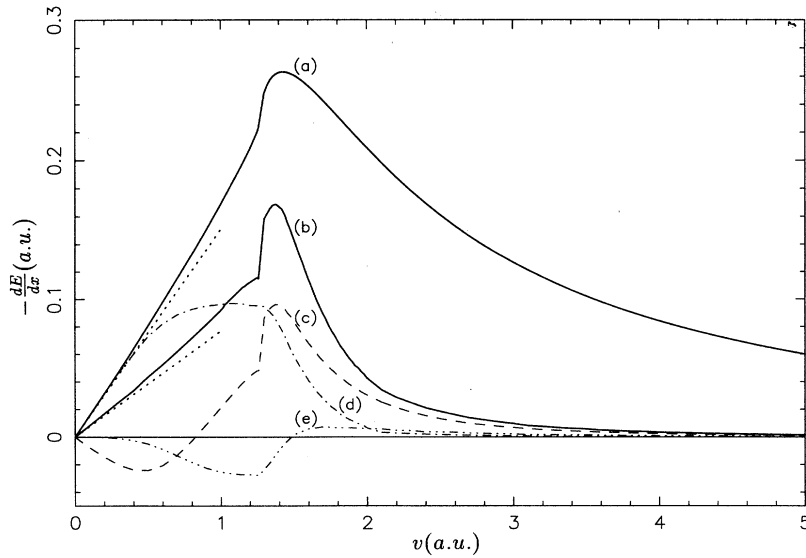


FIG. 10. Full RPA contributions to the stopping power calculated from Eq. (4.13), for $Z_1 = 1$ and $r_s = 2.07$, as a function of the velocity of the projectile. Solid curves labeled (a) and (b) represent Z_1^2 and Z_1^3 contributions, respectively, in atomic units. Z_1^3 contributions from f_1 , f_2 , and f_3 of Eqs. (4.14), (4.15), and (4.16) are plotted separately by lines labeled (c), (d), and (e), respectively. Z_1^2 and Z_1^3 contributions to the low-velocity limit of Eq. (4.23) are represented by dotted lines.

so-called static electron gas approximation can be made, and it follows from this approximation that only f_1 of Eq. (4.14) contributes to the Z_1^3 stopping power, as shown in the preceding section.

The static electron gas and plasmon-pole approximations to the Z_1^3 effect are plotted in Fig. 11, again for $r_s = 2.07$, as a function of the velocity of the projectile. The dashed and dashed-dotted lines labeled (b) and (d) represent the results obtained from Eq. (4.35) with the Z_1^3 term of Eq. (4.37), in the static electron gas and plasmon-pole approximations, respectively, and the dotted line, the result obtained for the Z_1^3 effect when the Z_1^3 term of Eq. (4.48), $(L_1)_{J-M}$, is introduced into Eq. (4.35). Both in the static electron gas and plasmon-pole approximations contributions to the Z_1^3 effect from f_2 and f_3 of Eqs. (4.15) and (4.16) are exactly equal to zero, and we compare, therefore, in this figure, these approximations with the full RPA contribution to the Z_1^3 effect coming from f_1 of Eq. (4.14), plotted by a solid line labeled (a). For comparison, the total Z_1^3 contribution to the stopping power is plotted in this figure by a solid line labeled (e), together with the corresponding results obtained in the static electron gas and plasmon-pole approximations, dashed and dashed-dotted lines, respectively.

It is obvious from this figure that at high velocities of the ion both the static electron gas approximation and twice the semiclassical formula of Jackson and McCarthy give a good account of the full RPA result, while at intermediate velocities this contribution is overestimated in these approaches, showing that the non-negligible zero-point motion of the electron gas gives rise to a smaller contribution from losses to one-step single excitations. However, this is almost compensated by the nonvanishing contribution from losses to two-step single excitations. As a consequence, the static electron gas approximation happens to be a good approximation of the full RPA result even at intermediate velocities, down to velocities

approaching the Fermi velocity of the electron gas, where the velocity distribution of target electrons is not negligible. This is exhibited in Fig. 12, where the total Z_1^3 contribution to the stopping power, represented in Fig. 10 by a solid line labeled (b), is plotted again together with the Z_1^3 contribution to the stopping power obtained after introduction of $(L_1)_{J-M}$ into Eq. (4.35).

The numerical results for the total RPA Z_1^3 contribution to the stopping power and different values of the electron density parameter r_s are illustrated in Fig. 13 by solid lines, together with the corresponding static electron gas approximation (dashed lines) and twice the formula of Jackson and McCarthy (dotted lines). At low velocities the Z_1^3 term gets larger as the electron density diminishes, and it becomes almost constant at the lower densities. On the other hand, at velocities higher than the Fermi velocity, where the static electron gas approximation is applicable, the magnitude of the Z_1^3 effect increases with r_s at high densities, and it decreases slowly at the lower densities. This is shown in Fig. 14, where the Z_1^3 term is plotted for different values of $x = 2m_e v^2 / \hbar \omega_p$, against the electron density parameter r_s .

The high-velocity limit of the Z_1^3 contribution to Eq. (4.35) with $(L_1)_{J-M}$, divided by $\sqrt{\omega_p}$, becomes velocity and density dependent through the parameter $x = 2m_e v^2 / \hbar \omega_p$, and this fact allows us, therefore, to plot a curve for the reduced Z_1^3 correction to the stopping power, $(-dE/dx) / \sqrt{\omega_p}$, that is independent of the electron density at high velocities of the projectile. Our full RPA calculation of this reduced Z_1^3 stopping power is exhibited in Fig. 15 for different values of r_s (solid lines), together with twice the result obtained by using the formula of Jackson and McCarthy, which is represented by a dotted line. At low velocities, where the stopping power is proportional to the velocity, the reduced Z_1^3 term increases with r_s , and it becomes almost independent of the electron density for metallic densities.

Finally, in order to account approximately for the Z_1^3

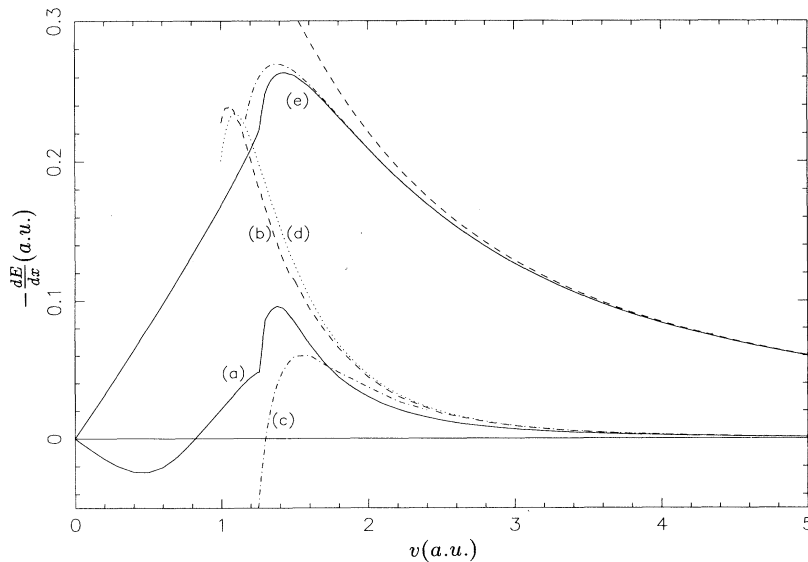


FIG. 11. Contribution to the Z_1^3 stopping power from f_1 of Eq. (4.14), as a function of the velocity of the projectile, for $Z_1 = 1$ and $r_s = 2.07$. (a) Full RPA result. (b) Static electron gas approximation. (c) Plasmon-pole approximation. (d) Result obtained after introduction of $(L_1)_{J-M}$ of Eq. (4.48) into Eq. (4.35). (e) Z_1^2 stopping power, as obtained in the full RPA (solid line), static electron gas approximation (dashed line), and plasmon-pole approximation (dashed-dotted line).

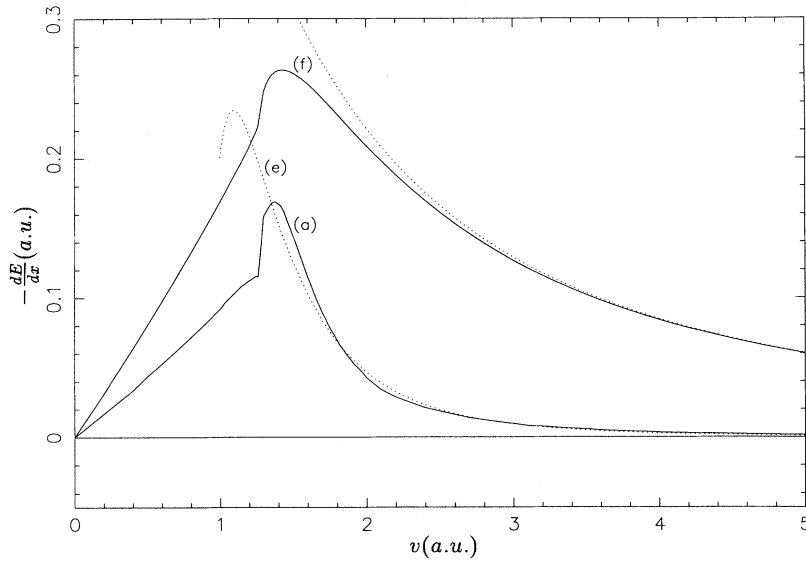


FIG. 12. Total Z_1^2 and Z_1^3 contributions to the stopping power, as a function of the velocity of the projectile, for $Z_1 = 1$ and $r_s = 2.07$. (a) Full RPA Z_1^3 stopping power. (e) Z_1^3 stopping power obtained after introduction of $(L_1)_{J-M}$ of Eq. (4.48) into Eq. (4.35); this is the same curve as curve labeled (d) in Fig. 11. (f) Full RPA Z_1^2 stopping power (solid line), together with the high-velocity limit obtained with the formula of Bethe, i.e., by introducing Eq. (4.42) into Eq. (4.35) (dotted line).

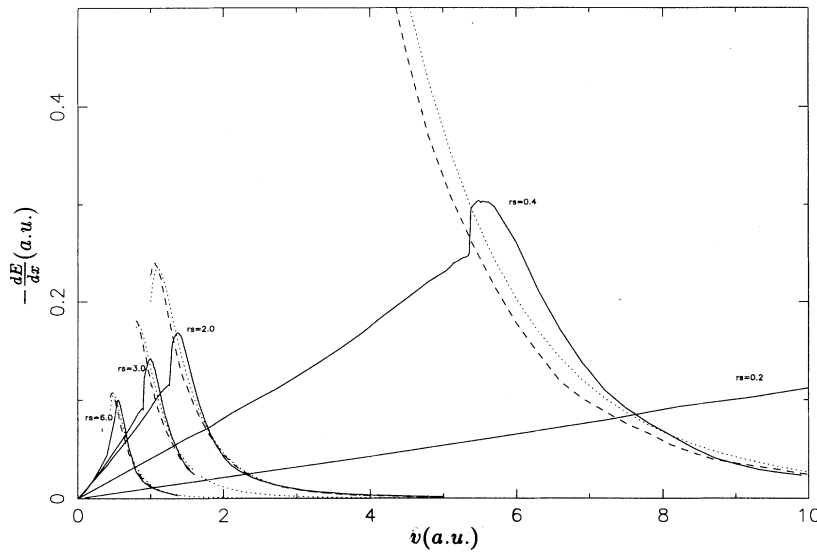


FIG. 13. Total Z_1^3 contribution to the stopping power, as a function of the velocity of the projectile, for $Z_1 = 1$ and 5 representative values of r_s : $r_s = 0.1$, $r_s = 0.4$, $r_s = 2.0$, $r_s = 3.0$, and $r_s = 6.0$. Results obtained after introduction into Eq. (4.13) of the full RPA response functions are plotted by solid lines. Dashed and dotted lines represent results obtained in the static electron gas approximation, and by introduction of $(L_1)_{J-M}$ of Eq. (4.48) into Eq. (4.35), respectively.

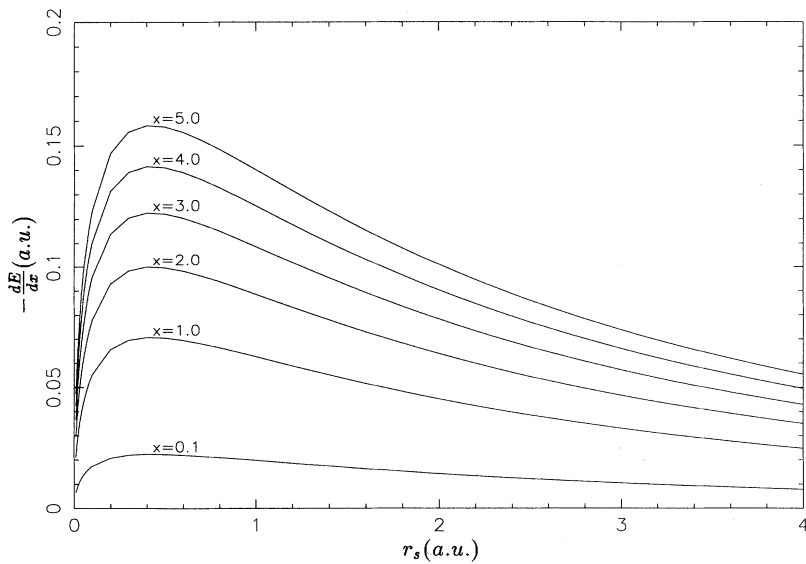


FIG. 14. Full RPA Z_1^3 contribution to the stopping power, as a function of r_s , for six representative values of $x = 2m_e v^2 / \hbar\omega_p$: $x = 0.1$, $x = 1.0$, $x = 2.0$, $x = 3.0$, $x = 4.0$, and $x = 5.0$.

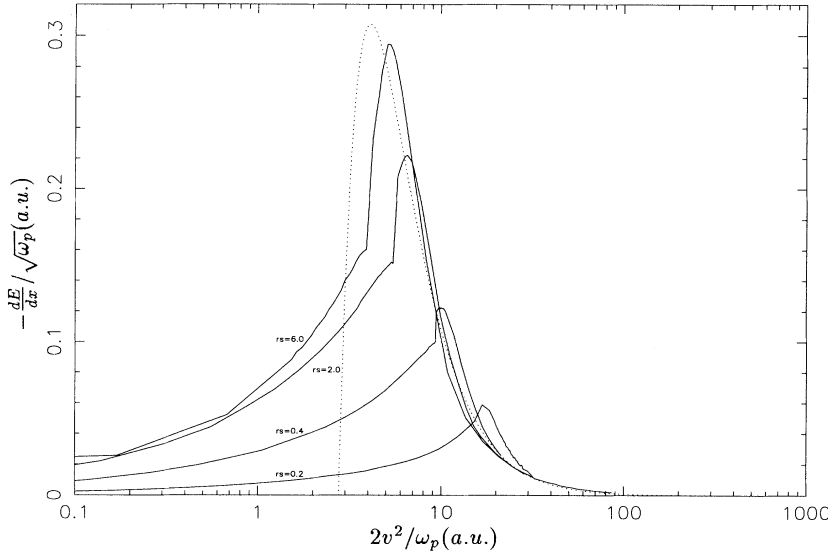


FIG. 15. Reduced Z_1^3 contribution to the stopping power, $(-dE/dx)/(\omega_p)^{1/2}$, as a function of $x = 2m_e v^2/\hbar\omega_p$, for $Z_1 = 1$ and 4 representative values of r_s : $r_s = 0.1$, $r_s = 0.4$, $r_s = 2.0$, and $r_s = 6.0$. Solid curves represent the result obtained in the full RPA, and the dotted curve, the result obtained after introduction of $(L_1)_{J-M}$ of Eq. (4.48) into Eq. (4.35), which is independent of the electron density.

effect coming from all target electrons, we have used a local plasma approximation. In this approximation, which has been used successfully to compute the Z_1^2 contribution to the stopping power of different materials,^{42,43} it is assumed that a local Fermi energy can be attributed to each element of the solid, and the effective Z_1^3 correction to the stopping power is computed, therefore, from the following expression:

$$\left(-\frac{dE}{dx}\right)^{(3)} = \frac{4\pi n Z_1^3 e^4}{m_e v^2} L_1^{\text{average}}, \quad (5.1)$$

where the Z_1^3 term, L_1 , is obtained after doing the average over each atom:

$$L_1^{\text{average}} = \frac{1}{Z_2} \int d^3 r n(\mathbf{r}) L_1[n(\mathbf{r})], \quad (5.2)$$

$n(\mathbf{r})$ represents the local density, which has been computed in the Hartree-Fock approximation by using the Wigner-Seitz boundary condition,⁴⁴ n is the total electron density, and Z_2 is the atomic number of the solid.

In Ref. 20 the Z_1^3 contribution to the stopping power of silicon, as computed in this way with the full RPA $L_1[n(\mathbf{r})]$ factor, has been presented, showing that at high enough velocities, for which all target electrons may be regarded as free, both the full RPA and the semiclassical results give a good account of the experimental result. However, at lower velocities the experimental Z_1^3 correction cannot be described by the semiclassical result, nor by results using the static electron gas or plasmon-pole approximation; indeed, it is easy to see from Fig. 13 that at the highest densities of the target, for which the local electron density parameter is $r_s \sim 0.2$, the static electron gas approximation would be applicable only for velocities higher than $v = 10v_0$, and, consequently, one needs to compute the full RPA response of the medium for the local plasma approximation to be applicable. One

sees that the results we obtain in this way are in good agreement with the experiment.

VI. CONCLUSIONS

First of all, we have developed a many-body perturbation theoretic scheme to derive the transition rate for processes leading, as a result of the passage of ions through matter, to all possible momentum transfers to the electron gas.

An alternative derivation of the imaginary part of the three-point Feynman diagram has been presented, and it has enabled us to give an explicit expression for the Z_1^3 correction to the stopping power in terms of both the real and the imaginary part of double and triple vertex functions.

Then, the Z_1^3 contribution to the stopping power has been evaluated, for the first time, in the full random-phase approximation, for a wide range of nonrelativistic velocities of the penetrating particle.

The previously studied low- and high-velocity limits have been discussed and their range of validity analyzed. We have shown that for velocities smaller than the Fermi velocity the stopping power is, up to third order in the ion charge, a linear function of the projectile velocity, and that in the high-velocity limit both the static electron gas approximation and twice the prediction of Ashley, Ritchie, and Brandt⁸ with the minimum impact parameter equal to the radius of the quantal harmonic oscillator give a good account of the full RPA result. We have, also, shown that the universality of the semiclassical formula for the Z_1^3 effect can be extended to our full RPA result.

Finally, we have demonstrated that our theory gives good agreement with experiment when the local plasma approximation is employed.

ACKNOWLEDGMENTS

The authors gratefully acknowledge discussions with E. Zaremba. We wish also to acknowledge the support of the University of the Basque Country, the Basque Unibertsitate eta Ikerketa Saila, the Spanish Comisión Asesora Científica y Técnica (CAICYT), and Iberdrola SA.

APPENDIX

The Z_1^3 contribution to the stopping power of Eq. (4.22), derived from the second-order wake potential of Eq. (4.21), may be represented as

$$\left(-\frac{dE}{dx}\right)^{(3)} = -2\frac{Z_1^3}{v\hbar^2} \int \frac{d^3q}{(2\pi)^3} \omega v_{\mathbf{q}} \int \frac{d^3q_1}{(2\pi)^3} v_{\mathbf{q}_1} v_{\mathbf{q}-\mathbf{q}_1} \times [f_1(\mathbf{q}, \omega, \mathbf{q}_1, \omega_1) + f_2(\mathbf{q}, \omega, \mathbf{q}_1, \omega_1) + f_3(\mathbf{q}, \omega, \mathbf{q}_1, \omega_1)] \theta(\omega), \quad (\text{A1})$$

where

$$f_1(q, q_1) = [\text{Im}(\epsilon_q^R)^{-1} \text{Re}(\epsilon_{q_1}^R)^{-1} \text{Re}(\epsilon_{q-q_1}^R)^{-1} + \text{Re}(\epsilon_q^R)^{-1} \text{Im}(\epsilon_{q_1}^R)^{-1} \text{Re}(\epsilon_{q-q_1}^R)^{-1} + \text{Re}(\epsilon_q^R)^{-1} \text{Re}(\epsilon_{q_1}^R)^{-1} \text{Im}(\epsilon_{q-q_1}^R)^{-1}] \text{Re}M_{q,q_1}^R, \quad (\text{A2})$$

$$f_2(q, q_1) = \text{Re}(\epsilon_q^R)^{-1} \text{Re}(\epsilon_{q_1}^R)^{-1} \text{Re}(\epsilon_{q-q_1}^R)^{-1} \times [H_{q,q_1}^R + H_{q_1,q}^R + H_{q-q_1,-q_1}^R], \quad (\text{A3})$$

$$f_3(q, q_1) = -[\text{Im}(\epsilon_q^R)^{-1} \text{Im}(\epsilon_{q_1}^R)^{-1} \text{Re}(\epsilon_{q-q_1}^R)^{-1} + \text{Im}(\epsilon_q^R)^{-1} \text{Re}(\epsilon_{q_1}^R)^{-1} \text{Im}(\epsilon_{q-q_1}^R)^{-1} + \text{Re}(\epsilon_q^R)^{-1} \text{Im}(\epsilon_{q_1}^R)^{-1} \text{Im}(\epsilon_{q-q_1}^R)^{-1}] \times [H_{q,q_1}^R + H_{q_1,q}^R + H_{q-q_1,-q_1}^R], \quad (\text{A4})$$

and

$$f_4(q, q_1) = -\text{Im}(\epsilon_q^R)^{-1} \text{Im}(\epsilon_{q_1}^R)^{-1} \text{Im}(\epsilon_{q-q_1}^R)^{-1} \text{Re}M_{q,q_1}^R, \quad (\text{A5})$$

all response functions being assumed to be retarded:

$$\epsilon_q^R = 1 - (\chi_q^0)^R v_q, \quad (\text{A6})$$

with

$$(\chi_q^0)^R = 2\hbar^{-1} \int \frac{d^3k}{(2\pi)^3} n_{\mathbf{k}} \left[\frac{1}{q^0 + \omega_{\mathbf{k}} - \omega_{\mathbf{k}+\mathbf{q}} + i\eta} - \frac{1}{q^0 - \omega_{\mathbf{k}} + \omega_{\mathbf{k}+\mathbf{q}} + i\eta} \right], \quad (\text{A7})$$

and

$$M_{q,q_1}^R = - \int \frac{d^3k}{(2\pi)^3} n_{\mathbf{k}} \left[\frac{1}{q^0 + \omega_{\mathbf{k}} - \omega_{\mathbf{k}+\mathbf{q}} + i\eta} \frac{1}{q_1^0 + \omega_{\mathbf{k}} - \omega_{\mathbf{k}+\mathbf{q}_1} + i\eta} + \frac{1}{-q^0 + \omega_{\mathbf{k}} - \omega_{\mathbf{k}+\mathbf{q}} - i\eta} \frac{1}{-(q^0 - q_1^0) + \omega_{\mathbf{k}} - \omega_{\mathbf{k}+\mathbf{q}-\mathbf{q}_1} - i\eta} + \frac{1}{-q_1^0 + \omega_{\mathbf{k}} - \omega_{\mathbf{k}+\mathbf{q}_1} - i\eta} \frac{1}{(q^0 - q_1^0) + \omega_{\mathbf{k}} - \omega_{\mathbf{k}-(\mathbf{q}-\mathbf{q}_1)} + i\eta} + (q_1 \rightarrow q - q_1) \right]. \quad (\text{A8})$$

The real part of M_{q,q_1}^R is invariant under the change $q^0 \rightarrow -q^0$, $q_1^0 \rightarrow -q_1^0$. For the imaginary part, we take advantage of the identity of Eq. (3.7), and find from Eq. (A8)

$$\text{Im}M_{q,q_1}^R = H_{q,q_1}^R + H_{q_1,q}^R + H_{(q-q_1),-q_1}^R, \quad (\text{A9})$$

where H_{q,q_1}^R is, as well as the imaginary part of the retarded function of Lindhard, $(\chi_q^0)^R$, an odd function of q^0 , and

$$H_{q,q_1}^R = \text{sgn}q^0 H_{q,q_1}^s, \quad (\text{A10})$$

H_{q,q_1}^s being the time-ordered function of Eq. (3.23), or, in terms of a sum over hole and particle states

$$H_{q,q_1}^R = (2\pi)^4 \text{P} \int \frac{d^3s}{(2\pi)^3} n_{\mathbf{s}} \int \frac{d^3p}{(2\pi)^3} (1 - n_{\mathbf{p}}) \delta^3(\mathbf{q} - \mathbf{p} + \mathbf{s}) \left[\frac{\delta(q^0 + \omega_{\mathbf{s}} - \omega_{\mathbf{p}})}{q_1^0 + \omega_{\mathbf{s}} - \omega_{\mathbf{s}+\mathbf{q}_1}} - \frac{\delta(q^0 - \omega_{\mathbf{s}} + \omega_{\mathbf{p}})}{-(q^0 - q_1^0) + \omega_{\mathbf{s}} - \omega_{\mathbf{s}+\mathbf{q}-\mathbf{q}_1}} \right]. \quad (\text{A11})$$

Now, we follow Esbensen¹² to decompose q^0 into $[q_1^0 + (q^0 - q_1^0)]$, and due to the symmetry with respect to the transformation $\mathbf{q}_1 \rightarrow \mathbf{q} - \mathbf{q}_1$ it can be easily shown that the same contributions from f_1 , f_2 , and f_3 of Eqs. (A2), (A3), and (A4) to the integral of Eq. (A1) come from

$$f_1'(q, q_1) = 2\text{Im}\epsilon_q^{-1} \text{Re}\epsilon_{q_1}^{-1} \text{Re}\epsilon_{q-q_1}^{-1} \text{Re}M_{q,q_1}, \quad (\text{A12})$$

$$f'_2(q, q_1) = 2\text{Re}\epsilon_q^{-1}\text{Re}\epsilon_{q_1}^{-1}\text{Re}\epsilon_{q-q_1}^{-1}H_{q, q_1}^s, \quad (\text{A13})$$

and

$$f'_3(q, q_1) = -4\text{Im}\epsilon_q^{-1}\text{Im}\epsilon_{q_1}^{-1}\text{Re}\epsilon_{q-q_1}^{-1}H_{q_1, q}^s, \quad (\text{A14})$$

respectively, while similar arguments can be used to show that f_4 of Eq. (A5) does not contribute to the integral. As a result, it is straightforward to conclude that Eqs. (4.13) and (4.22), derived from an open diagrammatic analysis of scattering matrix elements on the one hand, and from the wake potential, on the other hand, are equivalent.

- ¹ H. A. Bethe, *Ann. Phys. (Leipzig)* **5**, 325 (1930).
- ² F. Bloch, *Ann. Phys. (Leipzig)* **16**, 285 (1933); *Z. Phys.* **81**, 363 (1933).
- ³ W. H. Barkas, W. Birnbaum, and F. M. Smith, *Phys. Rev.* **101**, 778 (1956); W. H. Barkas, N. J. Dyer, and H. H. Heckman, *Phys. Rev. Lett.* **11**, 26 (1963); **11**, 138(E) (1963).
- ⁴ H. H. Andersen, H. Simonsen, and H. Sorensen, *Nucl. Phys. A* **125**, 171 (1969).
- ⁵ H. H. Andersen, J. F. Bak, H. Knudsen, and B. R. Nielsen, *Phys. Rev. A* **16**, 1929 (1977).
- ⁶ L. H. Andersen, P. Hvelplund, H. Knudsen, S. P. Moller, J. O. P. Pedersen, E. Uggerhoj, K. Elsener, and E. Morenzoni, *Phys. Rev. Lett.* **62**, 1731 (1989).
- ⁷ R. Medenwaldt, S. P. Moller, E. Uggerhoj, T. Worm, P. Hvelplund, H. Knudsen, K. Elsener, and E. Morenzoni, *Nucl. Instrum. Methods* **58**, 1 (1991); *Phys. Lett. A* **155**, 155 (1991).
- ⁸ J. C. Ashley, R. H. Ritchie, and W. Brandt, *Phys. Rev. B* **5**, 2393 (1972); **8**, 2402 (1973); **10**, 737 (1974).
- ⁹ N. Böhr, *Philos. Mag.* **25**, 10 (1913); **30**, 581 (1915).
- ¹⁰ K. W. Hill and E. Merzbacher, *Phys. Rev. A* **9**, 156 (1974).
- ¹¹ J. Lindhard, *Nucl. Instrum. Methods* **132**, 1 (1976).
- ¹² H. Esbensen, Ph.D. thesis, University of Aarhus, 1977.
- ¹³ C. C. Sung and R. H. Ritchie, *Phys. Rev. A* **28**, 674 (1983).
- ¹⁴ C. D. Hu and E. Zaremba, *Phys. Rev. B* **37**, 9268 (1988).
- ¹⁵ H. Mikkelsen and P. Sigmund, *Phys. Rev. A* **40**, 101 (1989).
- ¹⁶ H. Esbensen and P. Sigmund, *Ann. Phys. (N.Y.)* **201**, 152 (1990).
- ¹⁷ J. M. Pitarke, R. H. Ritchie, and P. M. Echenique, *Nucl. Instrum. Methods B* **79**, 209 (1993).
- ¹⁸ A. Arnau and E. Zaremba, *Nucl. Instrum. Methods B* **90**, 32 (1994).
- ¹⁹ J. J. Dorado, O. H. Crawford, and F. Flores, *Nucl. Instrum. Methods B* **93**, 175 (1994); **95**, 144 (1995).
- ²⁰ J. M. Pitarke, R. H. Ritchie, P. M. Echenique, and E. Zaremba, *Europhys. Lett.* **24**, 613 (1993).
- ²¹ G. Basbas, *Nucl. Instrum. Methods B* **4**, 227 (1984).
- ²² H. Bichsel, *Phys. Rev. A* **41**, 3642 (1990).
- ²³ T. D. Schultz, *Quantum Field Theory and the Many Body Problem* (Gordon and Breach, New York, 1964); A. L. Fetter and J. D. Walecka, *Quantum Theory of Many-Particle Systems* (McGraw-Hill, New York, 1971).
- ²⁴ J. Hubbard, *Proc. Phys. Soc. London* **243**, 336 (1957).
- ²⁵ J. Lindhard, *K. Dan. Vidensk. Selsk. Mat.-Fys. Medd.* **28** (8), 1 (1954).
- ²⁶ R. H. Ritchie, *Phys. Rev.* **114**, 644 (1959).
- ²⁷ R. Cenni and P. Saracco, *Nucl. Phys. A* **487**, 279 (1988). A minus sign in front of \cos^{-1} in Eq. (30) of this reference is missing, as pointed out in a subsequent paper [R. Cenni, F. Conte, A. Cornacchia, and P. Saracco, *Riv. Nuovo Cimento* **15** (12), 1 (1992)].
- ²⁸ Both M_{q, q_1} and H_{q, q_1} defined in Ref. 20 represent the retarded counterparts of the symmetrized time-ordered functions of Eqs. (3.22) and (3.23) (see the Appendix). Also, the coefficient in front of the left bracket of Eq. (7) in Ref. 20 represents a misprint and should, therefore, be removed.
- ²⁹ P. Lloyd and S. A. Sholl, *J. Phys. C* **1**, 1620 (1968). In terms of the notation of this reference, we find $M_{\mathbf{q}, 0; \mathbf{q}_1, 0} = -12g(\mathbf{q}, -\mathbf{q}_1, -\mathbf{q} + \mathbf{q}_1)$.
- ³⁰ P. M. Echenique, F. Flores, and R. H. Ritchie, in *Solid State Physics: Advances in Research and Applications*, edited by E. H. Ehrenreich and D. Turnbull (Academic, New York, 1990), Vol. 43, p. 229.
- ³¹ J. M. Pitarke, A. Bergara, and R. H. Ritchie, *Nucl. Instrum. Methods B* **99**, 87 (1995); A. Bergara and J. M. Pitarke, *ibid.* **96**, 604 (1995).
- ³² In the full expression for the Z_1^3 contribution to the stopping power given by Eq. (2.12) in Ref. 14, the dielectric functions corresponding to the frequencies ω_2 and ω_3 are advanced rather than retarded, and the quadratic response function has the frequency variables in the form $\omega_1 + i\eta$, $\omega_2 - i\eta$ and $\omega_3 - i\eta$. However, after transforming variables according to $\mathbf{q}_1 \rightarrow \mathbf{q}$, $\mathbf{q}_2 \rightarrow -\mathbf{q}_1$, and $\mathbf{q}_3 \rightarrow -(\mathbf{q} - \mathbf{q}_1)$, Eq. (2.12) in Ref. 14 is exactly equivalent to Eq. (4.22) of this paper, where the dielectric functions corresponding to the frequencies $\omega_1 = -\omega_2$ and $(\omega - \omega_1) = -\omega_3$ are retarded and the quadratic response function has the frequency variables in the form $\omega + i\eta$, $\omega_1 + i\eta$, and $(\omega - \omega_1) + i\eta$. The argument given in Ref. 12 that only one of the dielectric function factors contributes to the stopping power is, therefore, correct, as shown in the Appendix.
- ³³ J. Lindhard and M. Winther, *K. Dan. Vidensk. Selsk. Mat. Fys. Medd.* **34** (4), 1 (1964).
- ³⁴ E. Fermi and E. Teller, *Phys. Rev.* **72**, 399 (1947).
- ³⁵ I. Nagy and P. E. Echenique (unpublished).
- ³⁶ P. M. Echenique, R. M. Nieminen, and R. H. Ritchie, *Solid State Commun.* **37**, 779 (1981); P. M. Echenique, R. M. Nieminen, J. C. Ashley, and R. H. Ritchie, *Phys. Rev. A* **33**, 897 (1986); J. C. Ashley, R. H. Ritchie, P. M. Echenique, and R. M. Nieminen, *Nucl. Instrum. Methods B* **15**, 11 (1986).
- ³⁷ P. Hohenberg and W. Kohn, *Phys. Rev.* **136**, B864 (1964); W. Kohn and L. J. Sham, *ibid.* **140**, A1133 (1965).
- ³⁸ J. M. Pitarke and R. H. Ritchie, *Nucl. Instrum. Methods B* **90**, 358 (1994).
- ³⁹ J. D. Jackson and R. L. McCarthy, *Phys. Rev. B* **6**, 4131 (1972). The Z_1^3 contribution to the electronic stopping power of an atom that is approximated by a harmonic oscillator with a frequency ω_0 is found in the nonrelativistic limit to be $Z_1^3(4\pi n Z_2 \omega_0 / v^5) I_1$.

[See, also, Ref. 8, where I_1 is tabulated and gives, in the high-velocity limit, $I_1 = -(3\pi/2) \ln(\omega_0 a_\omega / v) - 2.4 \approx -(3\pi/2) \ln(5v/8a_\omega \omega)$, although Jackson and McCarthy give $I_1 = -(3\pi/2) \ln(3v/8a_\omega \omega)$]. If one equals, following Jackson and McCarthy, the so-called minimum impact parameter, a_ω , to the radius of the quantal harmonic oscillator, then one finally finds for the Z_1^3 term, L_1 , the result of Eq. (4.48), after replacing nZ_2 by the density of valence electrons and ω_0 by the plasma frequency of the electron gas, ω_p , and multiplying by 2.

⁴⁰ B. I. Lundqvist, *Phys. Kondens. Mater.* **6**, 206 (1967).

⁴¹ I. Nagy, A. Arnau, P. M. Echenique, and E. Zaremba, *Phys. Rev. B* **40**, 11 983 (1989).

⁴² J. Lindhard and M. Scharff, *K. Dan. Vidensk. Selsk. Mat. Fys. Medd.* **27** (15), 1 (1953).

⁴³ C. J. Tung, J. C. Ashley, and R. H. Ritchie, *Surf. Sci.* **81**, 427 (1979).

⁴⁴ T. C. Tucker, L. D. Roberts, C. W. Nestor, T. A. Carlson, and F. B. Malik, *Phys. Rev.* **178**, 988 (1969).